The 1993 Superstorm Cold Surge: Frontal Structure, Gap Flow, and Tropical Impact

DAVID M. SCHULTZ,* W. EDWARD BRACKEN, LANCE F. BOSART, GREGORY J. HAKIM, MARY A. BEDRICK,† MICHAEL J. DICKINSON, AND KEVIN R. TYLE#

Department of Atmospheric Science, State University of New York at Albany, Albany, New York

(Manuscript received 22 January 1996, in final form 28 June 1996)

ABSTRACT

In the wake of the eastern United States cyclone of 12–14 March 1993, a cold surge, originating over Alaska and western Canada, brought northerlies exceeding 20 m s^{-1} and temperature decreases up to 15°C over 24 h into Mexico and Central America. This paper addresses the multiscale aspects of the surge from the planetary scale to the mesoscale, focusing on 1) the structure and evolution of the leading edge of the cold surge, 2) the reasons for its extraordinary intensity and equatorward extent, and 3) the impact of the surge on the Tropics, specifically, on the strength of the trade winds and on the sea surface temperature in the eastern Pacific.

The cold surge was initiated as a developing cyclone over the Gulf of Mexico, and an upstream anticyclone east of the Rockies caused an along-barrier pressure gradient to form, forcing topographically channeled northerlies along the Rocky and Sierra Madre Mountains to transport cold air equatorward. On the mesoscale, the leading edge of the cold surge possessed nonclassical frontal structure. For example, as the cold surge entered Mexico, the coldest air and the strongest wind arrived at about 900 hPa before affecting the surface, suggestive of a tipped-forward leading edge to the surge. Also, satellite imagery and surface observations indicate that the leading edge appeared to be successively regenerated in the warm presurge air. The cold surge had characteristics reminiscent of a Kelvin wave, a tipped-forward cold front, a pressure-jump line, a bore, and a gravity current, but none of these conceptual/dynamical models was fully applicable. Associated with the cold surge, gap winds up to 25 m s^{-1} were observed in the Gulfs of Tehuantepec (a *tehuantepecer*), Fonseca, Papagayo, and Panama, owing to the strong cross-mountain pressure gradient. In the case of the tehuantepecer, a rope cloud emanated from the Isthmus of Tehuantepec and turned anticyclonically, consistent with an inertial oscillation.

On the synoptic and planetary scales, the extraordinary equatorward extent of the cold surge was aided by topographic channeling similar to cold-air damming, by a low-latitude upper-tropospheric trough, and by the lower branch of the secondary circulation associated with a confluent jet-entrance region aloft. The cold surge also impacted the tropical atmosphere and ocean, by contributing to the strengthening of the northeast trade winds over the eastern Pacific Ocean and by inducing local cooling of the sea surface temperature in the Gulfs of Tehuantepec and Papagayo by about 4°–8°C.

1. Introduction

a. Background

A dramatic example of the interaction between the Tropics and the midlatitudes is cold fronts from the central United States that penetrate into Mexico and Central America. These surges of cold air are associated with anticyclones that often occur in the wake of cyclogenesis east of the Rocky or Sierra Madre Mountains and can bring strong gusty northerly winds up to 30 m s^{-1}, air temperature decreases of 15°C in 24 h, persistent low clouds, and heavy precipitation on east- and north-facing slopes in Mexico and Central America. Because of their frequent occurrence during winter, cold surges are important forecast problems for this region. Their effects can last from one day to nearly two weeks after frontal passage (Reding 1992). The cold air can have drastic consequences on agriculture in Mexico (e.g., Garcia 1996), and the strong gusty winds are dangerous to ships in the Gulfs of Tehuantepec (Hurd 1929) and Panama (Frankenfield 1917; Chapel 1927). For the purpose of this paper, a *Central American cold surge*[1] (or

*Current affiliation: NOAA/National Severe Storms Laboratory, Norman, Oklahoma.

†Current affiliation: Aeromet, Inc., Kwajalein, Republic of the Marshall Islands.

#Current affiliation: General Sciences Corporation, Laurel, Maryland.

Corresponding author address: David M. Schultz, NOAA/National Severe Storms Laboratory, 1313 Halley Circle, Norman, OK 73069. E-mail: schultz@atmos.albany.edu

[1] As discussed by Davis (1995, p. 1762), the term *front* suggests a long-lived feature characterized by primarily balanced dynamics, whereas *surge* indicates a transient, largely unbalanced feature. It is beyond the purpose of this paper to definitively address the degree

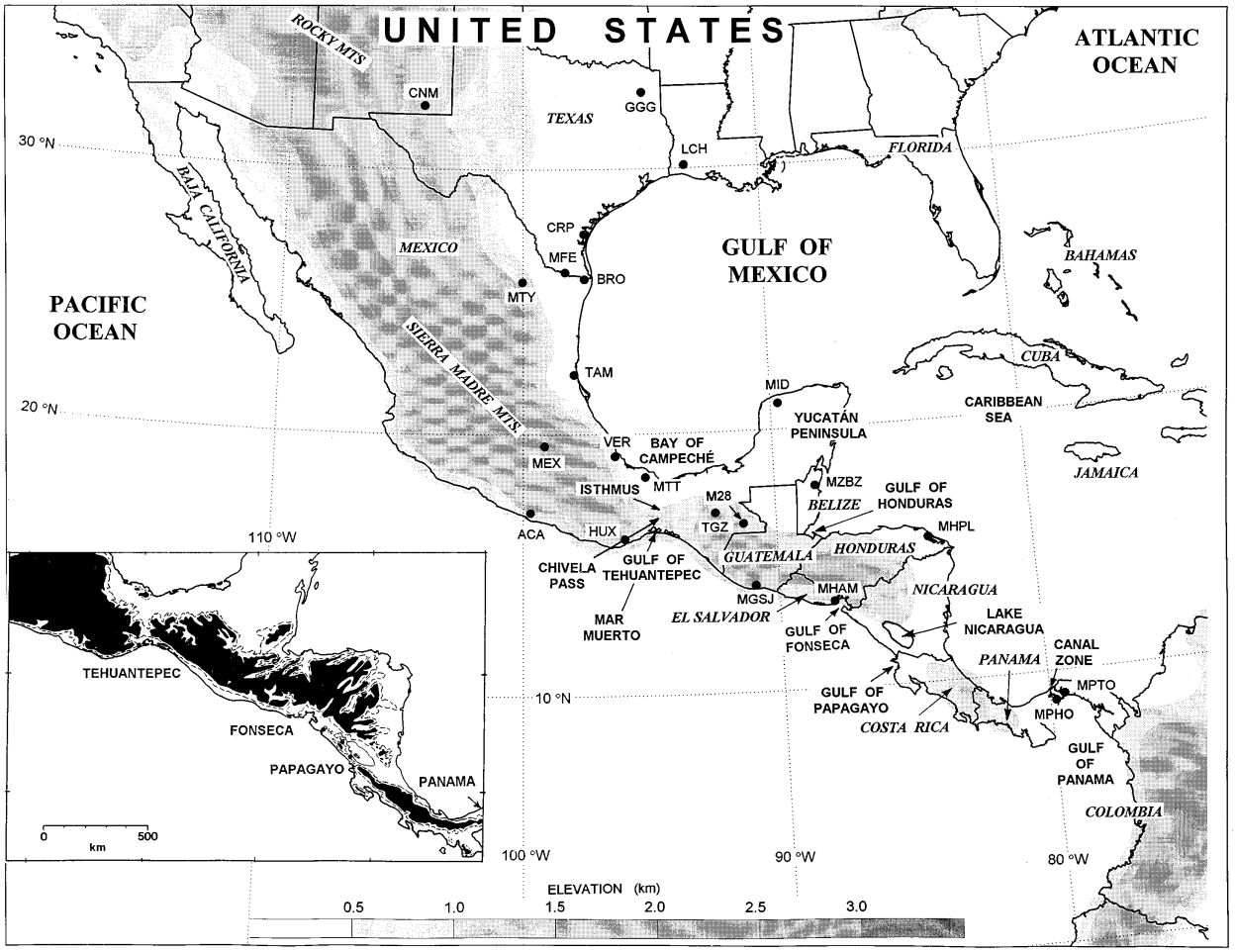

FIG. 1. Map illustrating the topography and geographical locations discussed in this paper. ECMWF (1.125° × 1.125° latitude–longitude resolution) topography over 500 m shaded according to legend. Insert: actual earth topography adapted from Clarke (1988, his Fig. 1) with locations of gulfs where gap wind events are commonly observed. Dashed line represents 200-m contour, and shaded areas are higher than 500 m. An important difference between the model and real topography is the Chivela Pass. The narrowness of this gap is not completely resolved by the ECMWF analyses; therefore, the model isthmus is higher and wider than the real isthmus is. M28 represents the location of an observation of a CACS on 6 April 1928, as reported by McBryde (1932).

CACS, see Reding 1992) will be defined as the leading edge of a cold anticyclone that originates poleward of Mexico and penetrates equatorward to at least 20°N. More specifically, the passage of a CACS will be identified by the onset of strong northerly flow at the surface (Colle and Mass 1995).

The interaction of cold fronts with the topography in Central America is crucial to their longevity (Hastenrath 1967). The geography of Mexico and Central America is dominated by the Sierra Madre Mountains (Fig. 1). Except for three major gaps in this mountain chain (Chivela Pass on the Isthmus of Tehuantepec, the gap at Lake Nicaragua near the Gulf of Papagayo, and the Panama Canal Zone on the Isthmus of Panama, and to a lesser extent the gap near the Gulf of Fonseca in Honduras), the Sierra Madre form a natural barrier to cold surges, separating the moist eastern coast and the dry western coast of Central America into two different climatological regions (Portig 1976, 423–424). Equatorward-moving cold air advances along the east side of the mountain chain, sometimes leaking through these gaps into western Central America. The most dramatic example of leakage occurs at the Isthmus of Tehuantepec, where the Bay of Campeché in the Gulf of Mexico lies approximately 220 km from the Pacific Ocean. The crest of the 40-km-wide Chivela Pass has an elevation of about 250 m above sea level, compared to the 2000-m peaks 50 km away. It is through this gap that cold air is funneled out over the Pacific Ocean. The power of these gap winds is demonstrated by a ship observation, 2.4 km offshore in the Gulf of Tehuantepec in February

of balance in this case owing to, in part, the sparseness of the data. Therefore, we will refer to Central American cold surges without the implications of the degree of balance.

1974, of 49.9 m s^{-1} winds with gusts to 60.2 m s^{-1} (Stumpf 1975a). Airborne sand reportedly caused extensive sandblasting of that ship.

Many names exist for the winds associated with CACSs. Generally, a *norte* or *norther* is simply a strong cold wind from the northwest to northeast (Huschke 1959). Other terms for this wind depend on the affected geographical area. A *chocolatero* or *chocolate gale* is a moderate norther in the gulf region of Mexico (Huschke 1959). A *tehuantepecer* (Hurd 1929) or *tehuano* (Trasviña et al. 1995) is a gap wind (e.g., Reed 1931; Overland and Walter 1981; Lackmann and Overland 1989; Mass et al. 1995; Dorman et al. 1995; also reviewed in Jackson and Steyn 1994) resulting from a norther in the Chivela Pass at the Isthmus of Tehuantepec that has been accelerated out over the Gulf of Tehuantepec. At other gaps of higher elevation, if the cold air on the east side is deep enough, then a foehn, or fall wind (Huschke 1959), may result as downslope winds dry out the western slopes. A *papagayo* or *popogaio* is a fall wind that results from a norther ascending the mountains in eastern Nicaragua and Guatemala and descending on the western slopes bringing cold, clear weather (Huschke 1959). It derives its name from the Gulf of Papagayo in northwestern Costa Rica, a Pacific Ocean inlet downwind of the gap in the mountains near the Lake District of Nicaragua. An *atemporalado* is a light persistent rain event in eastern Honduras after the passage of a cold front (Lessmann 1964; Ladd and Henry 1980; Reding 1992). Should the norther make it to northern Venezuela, it is then referred to as *el invierno de las chicharras* (the winter of the cicadas) since the sound of the cicadas is first heard during the second week of March, when these events typically occur (Goldbrunner 1963; Snow 1976, p. 345).

b. Motivation

This work grew out of a multiscale analysis of the snowstorm of 12–14 March 1993 on the east coast of the United States (Superstorm '93, also known as "the storm of the century," hereafter SS93). This intense midlatitude cyclone directly impacted eastern North America from the Caribbean to Canada (Hsu 1993; Walker 1993; DeAngelis et al. 1993; Gilhousen 1994; National Weather Service 1994; Kocin et al. 1995; Alfonso and Naranjo 1996). Besides blizzard conditions with heavy snowfall (exceeding 75 cm in some locations), a prefrontal squall line spawned tornadoes over Florida and caused the most widespread wind damage ever known in Cuba outside of a tropical storm (Alfonso and Naranjo 1996). Also, the winds associated with SS93 were responsible for a destructive 1.5–4-m storm surge in Florida (National Weather Service 1994; Kocin et al. 1995).

Our investigation of this storm was initially motivated by its exceptional intensity over the Gulf of Mexico, the important role that convection played in the incipient cyclogenesis, the planetary-scale antecedent conditions, the merger of two short-wave troughs in the westerlies contributing to the extreme cyclogenesis [in a manner similar to that described by Hakim et al. (1995, 1996) for the Cleveland superbomb of 25–26 January 1978], and the failure of the National Meteorological Center (NMC, now known as the National Centers for Environmental Prediction) models to predict the initial cyclogenesis in the Gulf of Mexico despite their successful forecasts of cyclogenesis 5 days in advance. These issues are examined in companion papers that discuss the planetary-scale (Bosart et al. 1996) and synoptic-scale (Dickinson et al. 1995) precursors to SS93. Other aspects of SS93 that have been addressed elsewhere include an overview of SS93 (Forbes et al. 1993; Kocin et al. 1995; Schumann et al. 1995), a pictorial of SS93 (*Weatherwise* 1995), an assessment of the NMC and research model performance (Uccellini et al. 1995; Caplan 1995; Huo et al. 1995; Dickinson et al. 1995), the importance of buoy data in the Gulf of Mexico to forecasting SS93 (Gilhousen 1994), the energetics of SS93 in the context of downstream development (Orlanski and Sheldon 1995), the structure and evolution of a mesoscale cold surge and snowband that developed over Colorado during the early stages of SS93 (Davis 1995), and the response of the National Weather Service to SS93 (National Weather Service 1994).

Further investigation of SS93 revealed that in its wake, cold continental air penetrated deep into the Tropics. Our primary motivation for this paper, itemized below, arises from observations about the cold surge associated with SS93 specifically and CACSs in general.

1) The 11-winter climatology of cases from 1979/80 through 1989/90 compiled by Reding (1992) indicates the surge associated with this case would rank tied for second among the most intense CACSs in terms of the southernmost extent of the surge (7°N) and the largest 48-h temperature decrease at Merida, Mexico (MID) (15°C). We wish to determine why this event was so unusually intense.
2) The nature of topographically trapped cold surges has been debated among many researchers [see, e.g., McInnes and McBride (1993), McBride and McInnes (1993), and Colle and Mass (1995) for reviews]. Suggested mechanisms to explain their dynamics include Kelvin waves, shelf waves, topographic Rossby waves (also called edge waves), topographically trapped gravity currents, and cold-air damming. It is of interest to compare the observations of the SS93 surge with these theories.
3) The fate of midlatitude cold fronts that approach tropical latitudes appears to be poorly understood (see section 6a). For example, Henry (1979, 1980) discussed some problems with frontal analysis in Central America. In addition, Horvath and Henry (1980) showed that during an eight-winter period, NMC analyzed only about half of the cold fronts that

had actually passed Belize. Some of the hypotheses for the fate of midlatitude cold fronts in the Tropics that have been proposed are that cold fronts lose their frontal properties and become shear lines, the pressure trough separates from the temperature gradient, fronts arrive first above the surface, and cold fronts never reach the Tropics.

4) As an example of extratropical–tropical interaction, cold surges contribute to the global energy transfer (Klaus 1973) and can act to increase the strength of the easterly trade winds (e.g., Riehl 1954, p. 273), resulting in greater convective activity within the Intertropical Convergence Zone (ITCZ) (e.g., Lessmann 1964). While these issues have been well documented for East Asian cold surges (see Lau and Chang 1987 for a review), there have been few studies on the impact of CACSs on the tropical atmosphere.

The remainder of this paper will be organized in the following manner. Readers familiar with cold surges and their impacts may wish to skip the literature review in section 2. Section 3 describes the data used for this study. Section 4 is a large-scale analysis of an exceptional cold-air outbreak associated with SS93, a major eastern United States cyclone, whereas section 5 examines the mesoscale structure and evolution of that event. Finally, sections 6 and 7 are a discussion and summary, respectively.

2. Previous research

a. Early studies

Beginning early in this century, Central American weather became paramount to the shipping community that used the recently completed Panama Canal as a shortcut in its travels. As noted by Frankenfield (1917), numerous ships and lives were lost in the 1800s and early 1900s near the Canal Zone owing to wintertime northers. He found that the approach of a norther was preceded by little barometric activity, but that a considerable rise in pressure usually followed. Frankenfield also identified four precursor weather patterns in the United States that suggested a means for forecasting Panamanian northers. His patterns were so general and varied, however, that they appear to have had little practical use at that time.

Chapel (1927) also discussed northers in Panama, apparently still unsure about their underlying cause. Editor A. J. Henry noted that some northers ''doubtless were occasioned by great anticyclones . . . which stretched from the Great Lakes southward to an indeterminate distance over the Gulf of Mexico''; but at the same time, the small scale (roughly 80 km) of the advancing pressure wave suggested that the disturbance was a localized phenomenon (Chapel 1927, p. 528). This discrepancy seems to have been resolved by Hurd (1929), who identified topographic channeling of anticyclones originating from the Great Plains of the United States as the ultimate cause of the gap winds across the Isthmus of Tehuantepec. In addition, Hurd (1929) recognized the difference between the northerlies in gradient wind balance associated with anticyclones over the Great Plains (gradient northers) and the topographically forced northerlies associated with tehuantepecers (derivative, overflow, or orographic northers). He also noted that the tehuantepecer was sometimes accompanied by an arc-shaped cloud band. During the early period of satellite observation and interpretation, Parmenter (1970) presented an example of this rope cloud associated with a tehuantepecer over the eastern Pacific Ocean. Later Simpson (1987, p. 40) showed that the distance traveled by Parmenter's rope cloud as a function of time was in agreement with analytical expressions for gravity currents.

McBryde (1932; 1942a, 259–261) discussed the weather associated with cold surges in southwest Guatemala, relating historical accounts and first-hand narrative. Goldbrunner (1963) presented examples of cold fronts that penetrated from North America into northern Venezuela. As noted by Snow (1976, p. 345), these fronts often produce heavy precipitation, resulting in flooding because of the poor ground cover and soil conditions along the Venezuelan slopes.

Bluestein (1977) showed that midlatitude cloud bands entering the Tropics tended to orient along the axis of dilatation of the synoptic-scale flow and to become embedded in a region where the resultant deformation was at a maximum. This work also helped explain the longevity of some equatorward-moving cloud bands from the midlatitudes once they had entered the Tropics. Fitzjarrald (1986) presented an example of the presurge environment near Veracruz, Mexico (VER), and showed that the height of the subsidence inversion associated with the wintertime subtropical high decreased prior to the arrival of a norther.

b. Climatology

There have been many attempts at compiling observations of rainfall and frontal passages in the tropical Americas: Spinden (1928), Portig (1965, 1976), and Hastenrath (1967) for Central America; DiMego et al. (1976) and Henry (1979) for the Gulf of Mexico and the Caribbean; *Weatherwise* (1963), Trewartha (1966), Hill (1969), Klaus (1973), and Mosiño Alemán and García (1974) for Mexico; Bosart and Schwartz (1979) for the Bahamas; Portig (1976) for the Caribbean Islands; Fermor (1971) for Jamaica; Garcia et al. (1978) for the Dominican Republic; Horvath and Henry (1980) for Belize; McBryde (1942a,b) for Guatemala; and Ladd and Henry (1980) for Honduras.

Because of the fluxes of heat and moisture over the warm waters of the Gulf of Mexico, which moisten and destabilize the cold air mass, and the orographically enhanced ascent on the windward side of the mountains,

flooding often occurs with CACSs (McBryde 1942a, p. 261). Heavy precipitation may also occur as fronts stall at their most equatorward extent in Central America (Portig 1965, p. 74). Although winter is generally considered the dry season for Central America, secondary maxima in precipitation for eastern locations often occur in December and January (Portig 1965, 76–78; Hastenrath 1967, p. 233), while western locations experience a true dry season during the winter. Although snow at sea level does not occur, hail can fall in March and April (McBryde 1942a, p. 261), apparently with the passage of late season CACSs.

As noted by Klaus (1973), Henry (1979), and Reding (1992), among others, the frequency of cold-frontal passages in Mexico and Central America varies considerably. Klaus's (1973) data for the winter period (September–April) for the years 1899–1960 indicate quite substantial interannual variability, ranging from 0 to 27 events per winter with an average of 13. For an 11-year period (1979–80 through 1989–90), Reding (1992, p. 28) found an average of 16 CACSs pass Merida, Mexico, each winter (October–March). For a 9-yr period (1969/70 through 1977/78), Horvath and Henry (1980) found an average of 10 events pass Belize (MZBZ) during winter (November–March). DiMego et al.'s (1976) wintertime frontal frequencies range from about eight a month for northern Mexico to less than one per month south of Honduras. Generally, these values are in agreement despite a variety of methodologies and datasets.

The studies described above also indicate that cold-frontal passages in Mexico and Central America tend to occur during the winter months with the maxima in frequency and intensity in January and February (Reding 1992, 30–32). The fronts have a tendency to remain tied to the Sierra Madre Mountains because of topographic channeling and heat fluxes over the Gulf of Mexico, which erode the cold air/high pressure behind the front (e.g., Colle and Mass 1995). Dallavalle and Bosart (1975), Hartjenstein and Bleck (1991), Mecikalski and Tilley (1992), Colle and Mass (1995), Tyle (1995), Garcia (1996), and Konrad (1996) discussed the synoptic flow typically associated with North American cold surges. They found that, in most cases, a high-amplitude upper-level ridge over the western United States was necessary for cold-air advection and anticyclonic-vorticity advection on the poleward side of the jet entrance region to favor anticyclogenesis. Often the equatorward advance of the anticyclone would be initiated by a mobile upper-level vorticity maximum. Hartjenstein and Bleck (1991) performed idealized model simulations, which indicated that cold air masses with large temperature contrasts are able to penetrate equatorward even with unfavorable southwesterly flow aloft. Cold air masses with more modest temperature contrasts, however, require relatively weak upper-level zonal flow or strong dynamical forcing in the form of upper-level ridging over the Rockies to reach far equatorward (see also Mecikalski and Tilley 1992).

Tropical cold surges are not limited to the Americas. There is abundant literature on Asian cold-air outbreaks as part of the winter monsoon (e.g., Ramage 1971, 157–161; Houze et al. 1981; Chang et al. 1983; Boyle and Chen 1987; Lau and Chang 1987; Ding 1994; Wu and Chan 1995). In the Southern Hemisphere, cold-frontal passages into the subtropics and Tropics have been discussed by, for example, Baines (1980) and Smith et al. (1995) for Australia; and Goldbrunner (1963), Myers (1964), Trewartha (1966, 42–49), Parmenter (1976), Prohaska (1976), Ratisbona (1976), and Fortune and Kousky (1983) for South America. Cold surges into tropical Africa are rare owing to the interior plateau inhibiting frontal advance inland (Taljaard 1972, p. 157).

Therefore, although not a rare occurrence, the cold surges that reach the Tropics happen often enough to imply a ''unity instead of dichotomy between tropical and midlatitude weather'' (Myers 1964, p. 520). In fact, few studies have investigated the effects of North American incursions after entering Mexico and Central America. Besides the sensible cooling and enhanced low cloudiness in the cold air, other more subtle impacts on the tropical environment may occur, such as a change in the strength of the trade winds, the location or strength of the ITCZ, cooling in the eastern Pacific Ocean, or even feedbacks to other phenomena such as El Niño–Southern Oscillation (ENSO).

c. Interaction between CACSs and the eastern Pacific Ocean

Strong winds acting upon the ocean surface can produce a variety of responses. For example, the initial surge may produce a transient response in the oceans in the form of surface waves radiating away from the impulse. Hurd (1929) noted that the swell from strong tehuantepecers had been known to reach the Galapagos Islands, 1600 km to the south. Alternatively, steady wind forcing may produce ocean currents.

Traditionally, ocean surface currents flow to the right of the wind in response to Ekman transport, a balance between the surface wind stress and the Coriolis force (e.g., Pond and Pickard 1983, 106–115). For a northerly wind blowing along the west coast of a continent (north–south-oriented coast), the westward Ekman transport of surface water causes ascent of cooler subsurface water (i.e., *upwelling*). Forcing on timescales shorter than the inertial period leads to direct transport of water in the same direction as the wind (e.g., storm surges). The impulsive forcing by strong gap winds on the ocean surface can produce a rapid response within the oceans, which may involve strong jetlike currents colloquially known as *squirts* (Ramp et al. 1991), or *supersquirts* (Barton et al. 1993) if they are several hundred kilo-

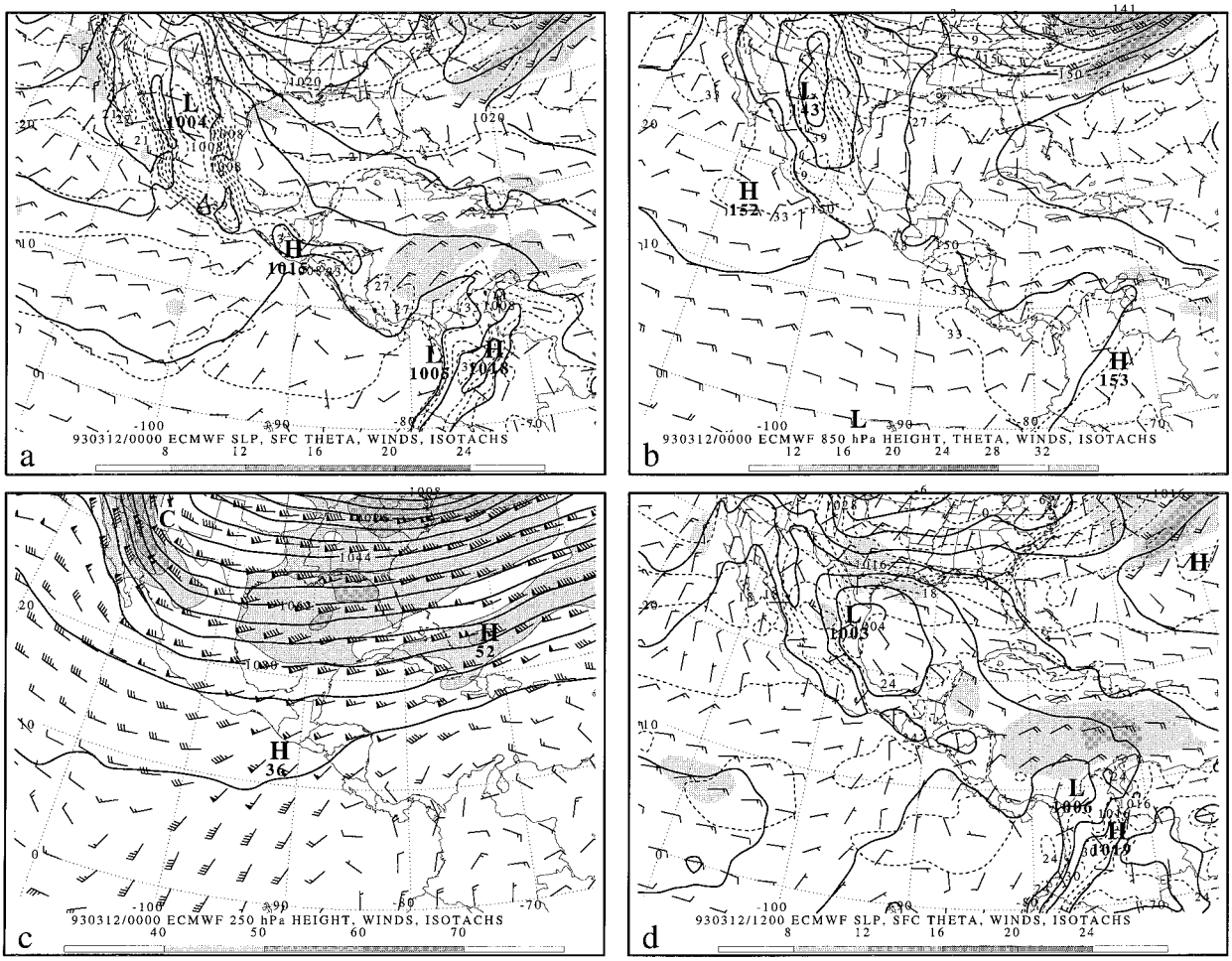

FIG. 2. ECMWF analyses. (a) 0000 UTC 12 March 1993: sea level pressure (solid lines every 4 hPa), surface potential temperature (dashed lines every 3°C), 10-m wind (one pennant, full barb, and half-barb denote 25, 5, and 2.5 m s^{-1}, respectively), and wind speed (m s^{-1}, shaded). (b) 0000 UTC 12 March 1993: 850-hPa geopotential height (solid lines every 3 dam), 850-hPa potential temperature (dashed lines every 3°C), 850-hPa wind [as in (a)], and wind speed (m s^{-1}, shaded). (c) 0000 UTC 12 March 1993: 250-hPa geopotential height (solid lines every 6 dam), 250-hPa wind [as in (a)], and wind speed (m s^{-1}, shaded). The ''C'' represents the location of potential vorticity anomaly C discussed in text. (d) Same as (a) except for 1200 UTC 12 March 1993.

meters in scale.[2] Coastal upwelling and the formation of anticyclonic–cyclonic gyre pairs on either side of the squirt are also possible (e.g., Flierl et al. 1983; Wang 1987; Clarke 1988; McCreary et al. 1989; Trasviña et al. 1995). Strong upwelling also bears important implications for oceanic biota and the fishing industry since strong chlorophyll anomalies indicate enhanced primary production in the cooler, nutrient-rich upwelled region (e.g., Barton et al. 1993). In fact, much of the early research on the oceanic effects of tehuantepecers remains as research reports published by the Intertropical Tuna Commission (G. Quiros Alvarez 1995, personal communication).

With the advent of satellite imagery, researchers were able to view sea surface temperatures (SSTs) with higher temporal and spatial resolution than before. Stumpf (1975a,b), Stumpf and Legeckis (1977), Legeckis (1986, 1988), Clarke (1988), Barton et al. (1993), and Clemente-Colón and Chang (1995) employed satellite imagery to show the effects of gap winds on the eastern Pacific Ocean. They found that the typical SST decrease associated with tehuantepecers was about 6°–12°C, agreeing with in situ measurements.

Recently, oceanographers have begun mounting field

[2] The term ''squirt'' became popular after the CODE/SuperCODE experiments and during the Coastal Transition Zone (CTZ) experiment off northern California (Ramp et al. 1991). It refers to the cold current jets that project offshore from the midlatitude upwelling zones into the California Current water. These squirts result from the convergence of currents associated with baroclinically unstable eddies that form in that region during the upwelling season. Currently, usage of this term for the oceanic response to gap wind events by oceanographers, therefore, denotes similarity in the kinematic sense, but not in the dynamic sense (D. B. Enfield 1995, personal communication).

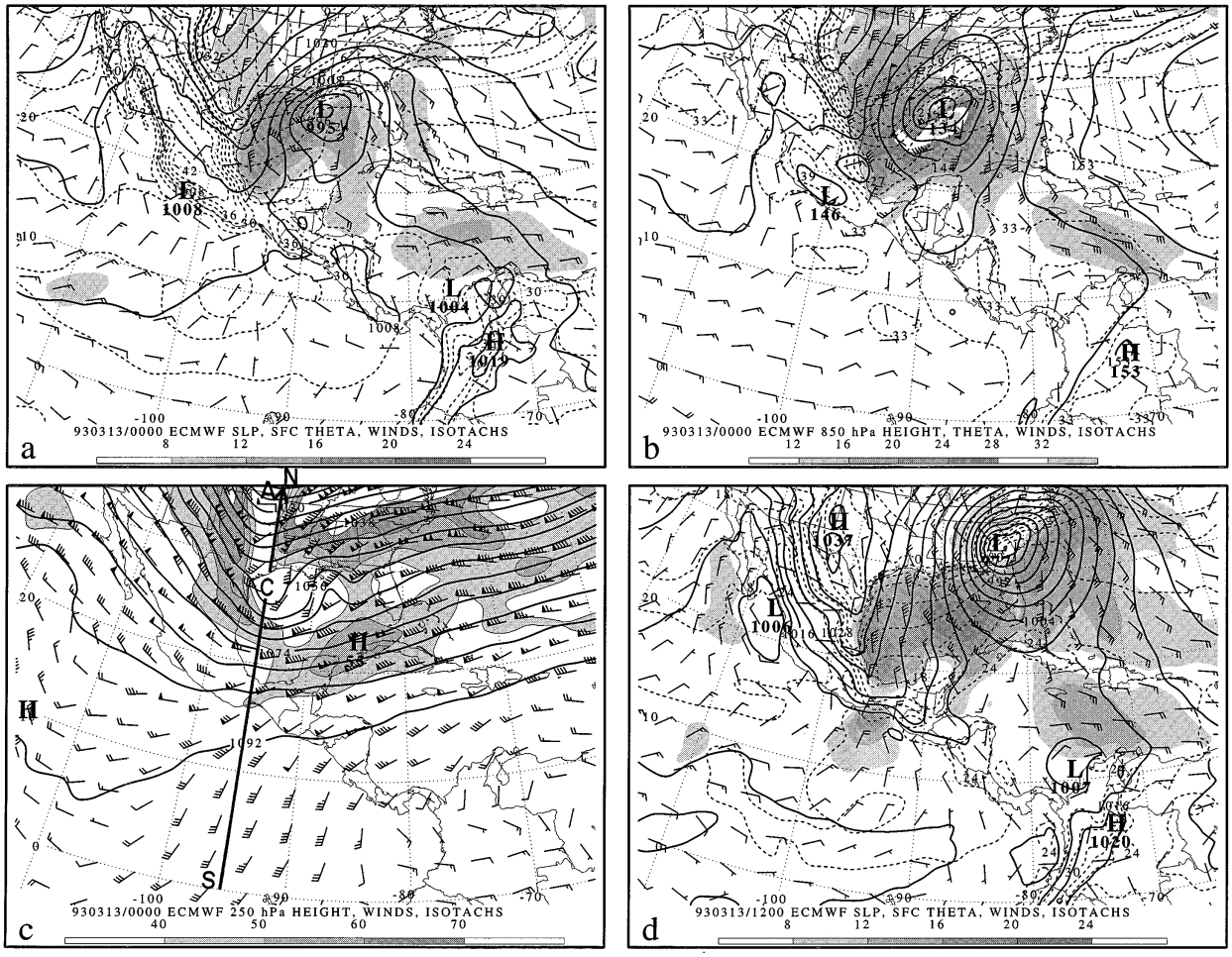

FIG. 3. Same as for Fig. 2 except 0000 UTC 13 March 1993 in (a), (b), and (c). (c) The ''A'' represents the location of potential vorticity anomaly A discussed in text. The location of cross section south–north (SN) from Fig. 4a identified by thick solid line. (d) Same as for Fig. 2a except 1200 UTC 13 March 1993.

programs to the Gulf of Tehuantepec to investigate the oceanic response to these wind impulses: Tehuano in 1989 (Barton et al. 1993; Trasviña et al. 1995) and Tehuano II in February 1996 (A. Trasviña 1995, personal communication). The results of these field programs show the detailed evolution of the upper ocean to the forcing from a tehuantepecer. In one case, Barton et al. (1993) noted an 8°C drop in SST within about 6 h after the onset of the strong northerly winds.

Roden (1961) considered the dynamics of the oceanic response to tehuantepecers in the eastern Pacific Ocean and showed that the mean wind and SST in the Gulf of Tehuantepec were closely related, suggesting that the cause was upwelling owing to tehuantepecers. Relating the curl of the wind stress to the horizontal mass divergence, Roden [1961, his Eq. (2)] calculated an average upwelling speed during a tehuantepecer to be 10 m day^{-1} acting on a timescale of a day and a half, substantially less than implied by later observational work (Stumpf and Legeckis 1977). Stumpf (1975b) noted that ship observations consistently indicated that the SST was 1°–2°C cooler than the air temperature in the core of the maximum wind; this implicated upwelling as the primary cooling mechanism as opposed to sensible or evaporative cooling. The Gulf of Tehuantepec may be particularly prone to upwelling, since it has a shallow thermocline and water of 22°C (6°–8°C colder than the surface water) 15–40 m under the surface (e.g., Stumpf and Legeckis 1977; Trasviña et al. 1995). Stumpf (1975b) concluded that winds associated with a tehuantepecer would be sufficient to mix this water upward. Field measurements indicated that sensible heat fluxes were unimportant during the initial cooling phase (Barton et al. 1993). Yet, despite these recent advances, many questions still persist about the interaction between the ocean and the atmosphere during CACSs; Barton et al. (1993, p. 30) summarize many of these concerns.

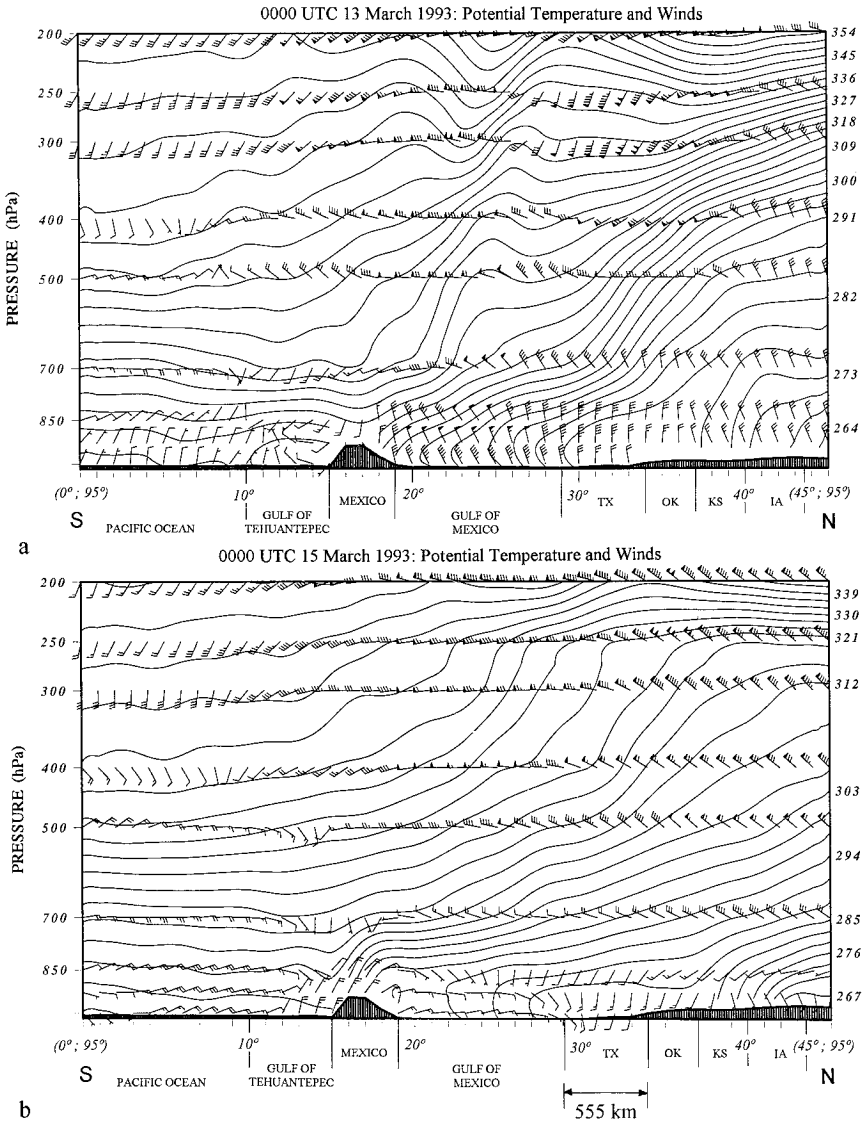

FIG. 4. Vertical cross sections through the cold surge: potential temperature (solid lines every 3 K) and wind (one pennant, full barb, and half-barb denote 25, 5, and 2.5 m s^{-1}, respectively). (a) 0000 UTC 13 March 1993: cross section south–north (NS) along 95°W from 0° to 45°N. Because of the resolution of the ECMWF analyses, the Isthmus of Tehuantepec is at a higher elevation in the model than it is on the real earth. (b) 0000 UTC 15 March 1993: same as (a). (c) 0000 UTC 15 March 1993: cross section west–east (WE) along 12.5°N from 110° to 70°W.

3. Data

The gridded analyses in section 4 come from the World Climate Research Programme/Tropical Oceans Global Atmosphere (WCRP/TOGA) Archive I of the European Centre for Medium-Range Weather Forecasts (ECMWF) uninitialized analyses (Trenberth 1992). These analyses were stored in spherical harmonic form with a horizontal resolution equivalent to 1.125° × 1.125° latitude–longitude, but were bilinearly interpolated to a 1° × 1° latitude–longitude grid at all mandatory levels from the surface to 10 hPa every 6 h.

The data employed in the mesoscale analyses contained in section 5 consist of the standard operational dataset of surface and upper-air observations. Domestic United States data were supplemented by Mexican and Central American hourly observations, international METAR reports, Comprehensive Ocean–Atmosphere Data Set (COADS) data (Woodruff et al. 1987), Tropical Oceans Global Atmosphere–Tropical Atmosphere Ocean (TOGA–TAO) array data (Hayes et al. 1991), and 6-h synoptic observations. Surface and upper-air data from Nicaragua were not available from any source. Satellite imagery was available in hard-copy form from the State University of New York at Albany (SUNYA)

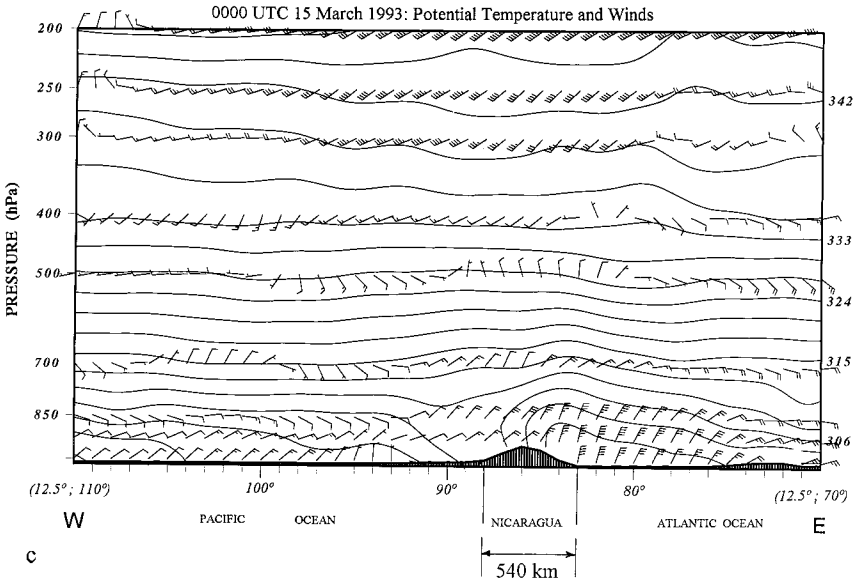

FIG. 4. (*Continued*)

archives and in digital form from the Space Science and Engineering Center (SSEC) at the University of Wisconsin—Madison. Precipitation data were obtained from the Global Center for Environmental Assessment Services (CEAS) (currently the Climate Prediction Center) summary via the National Center for Atmospheric Research (NCAR).

4. Large-scale analysis

In this section, the large-scale analysis of the CACS associated with SS93 based upon the ECMWF analyses is presented. The rationale for using ECMWF global analyses is that the synoptic and meso-α scale[3] structure of the surge was captured owing to strong synoptic-scale forcing in a region of large topographical relief. The structure of the ITCZ and tropical meso-β-scale features, on the other hand, were generally poorly resolved. For convenience, the evolution of the cold surge is examined in three stages: initiation, maturity, and decay.

a. Initiation of the cold surge: 0000 UTC 12 March–0000 UTC 13 March 1993

The large-scale analysis of the cold surge associated with SS93 during its developing phase, 0000 UTC 12 March 1993 (hereafter 12/00) to 13/00, is presented in Figs. 2–3a–c. At 12/00, a 1004-hPa northwest–southeast-elongated sea level pressure center was developing over northern Mexico (Fig. 2a) in response to the approaching short-wave trough [potential vorticity (PV) anomaly C in Bosart et al. (1996, their Fig. 3)] in northwestern Mexico at upper levels (Fig. 2c). Later, PV anomaly C approached the base of the deepening planetary-scale trough, causing the surface low to move southeastward and deepen 8 hPa in the 12-h period ending 13/00 (Figs. 2d and 3a). By 13/12, the short-wave trough associated with PV anomaly C, situated in the southern branch of the jet stream over the western Gulf of Mexico, was joined by a short-wave trough in the northern branch of the jet over Oklahoma (PV anomaly A in Bosart et al. 1996, their Fig. 3). These two PV anomalies were brought together within the large-scale confluent flow and rotated around each other within the larger scale trough over the central United States (Fig. 3c). This situation was quite favorable for the eventual merger of the two anomalies, as shown by Hakim et al. (1995, 1996) for the Cleveland superbomb.

An approximately 20 m s^{-1} cross-equatorial 250-hPa flow over the eastern Pacific (85°–100°W) fed into a broad confluent region over the Gulf of Tehuantepec (e.g., Figs. 2c and 3c). Although a climatological feature of the upper-level flow (see, e.g., Peixoto and Oort 1992, p. 151), the confluence was much stronger for this case. Riehl (1954, p. 273) and Newton (1965) noted the correspondence between a strong, subtropical jet stream and a low-latitude polar outbreak and, as will be shown later for the cold surge associated with SS93, the anomalously confluent flow over Central America appeared to be important to the unusual strength and low-latitude extent of the cold surge.

Lower-tropospheric cold air associated with an anticyclone in the central United States was situated north of the cyclone center (Kocin et al. 1995, their Fig. 3a). The anticyclone originated over Alaska and western

[3] Meso-α and meso-β represent characteristic length scales of 200–2000 km and 20–200 km, respectively (Orlanski 1975).

Canada, was joined by an eastward-moving anticyclone coming from the Gulf of Alaska on 10–11 March, and intensified (Bosart et al. 1996, their Figs. 10c and 11c). The initiation of the cold surge appeared to be related to the eastward movement of SS93 and the reorganization of the isobars in northern Texas from an orientation nearly parallel to the Rockies at 12/00 to perpendicular to the Rockies at 12/12 (cf. Figs. 2a and 2d). This rearrangement caused the wind near the mountains to become terrain-parallel, much like cold-air damming east of the Appalachian Mountains (e.g., Richwien 1980; Bell and Bosart 1988). The initiation of the cold surge is consistent with the results of Colle and Mass (1995), who attributed the onset of a specific cold-surge event to a change in the orientation of the isobars relative to the topography. The reorientation then caused a terrain-parallel northerly component to the wind, but the Coriolis force produced an upslope component, resulting in the development of a structure similar to cold-air damming. The flow then became more parallel to the terrain (e.g., the flow over Texas in Figs. 2d and 3a), a consequence of antitriptic balance parallel to the mountain range and geostrophic balance normal to the range.

As the cold surge progressed equatorward on 13/00, the leading edge was located just south of Veracruz, Mexico (VER), on the north side of the Isthmus of Tehuantepec, directly under the 250-hPa jet-entrance region (Figs. 3a–c). Twenty-four-hour sea level pressure rises behind the cold surge range from typical values of 10 hPa $(24\ h)^{-1}$ at Brownsville, Texas (BRO), to a maximum of over 24 hPa $(24\ h)^{-1}$ near Carlsbad, New Mexico (CNM). Surface wind speeds of 20 m s^{-1} from the ECMWF analyses are consistent with the observed winds along the Mexican coast (cf. Figs. 3a and 11b).

A vertical cross section at 13/00 through the cold surge along 95°W (the longitude of Chivela Pass) is shown in Fig. 4a. It is apparent that the leading edge of the surge is associated with north-northwesterly winds and a strong potential temperature gradient connected to the deep baroclinic structure of the jet farther north. The cold surge and its associated northerlies were a deep phenomenon, extending up through 700 hPa over the Gulf of Mexico (Fig. 4a). The cold advection associated with the surge, in the presence of a warm lower boundary, created an absolutely unstable layer just above the earth's surface, despite (presumably) strong mixing, which tended to bring the near-surface layer toward more neutral stability (Fig. 4b). Therefore, in this cross section, the coldest air and core of the strongest wind along the leading edge of the surge appeared to be tipped forward, moving in at 925 hPa before the surface.

Further south, a jet of low-level easterlies north of Venezuela impacted the east coasts of Panama and Costa Rica (Figs. 2a,b), strengthening to about 10 m s^{-1} by 12/12 (Fig. 2d). There are indications that this jet was baroclinic as the winds turned clockwise (veered) with height. This feature appeared to be a localized maximum of the northeast trade winds (Peixoto and Oort 1992, their Fig. 7.1), another maximum of which is seen near 7°N, 110°W (Fig. 2d). Antecedent cold surges during the previous two weeks (Bosart et al. 1996, their Fig. 15) and their accompanying anticyclones may also possibly account for the strength of these easterlies. By 13/00, the easterlies north of South America began to veer, apparently in response to the approaching upper-level trough and low-level frontal zone (Figs. 3b,c).

b. Maturation of the cold surge: 1200 UTC 13 March–1200 UTC 14 March 1993

The evolution of the cold surge during its mature stage is illustrated at 13/12 (Fig. 3d), 14/00 (Fig. 5), and 14/12 (Fig. 6a). At 13/12, the hazardous weather associated with the prefrontal squall line was affecting Florida and Cuba with heavy rain, 25 m s^{-1} winds, and tornadoes (e.g., National Weather Service 1994; Kocin et al. 1995; Alfonso and Naranjo 1996). Meanwhile, the 1037-hPa surface anticyclone from the United States moved farther equatorward along the eastern slope of the Rocky Mountains (Fig. 3d). By 14/12, the center of the surface anticyclone, following in the path of SS93, headed toward the southeast United States (Fig. 6a) as the upper-level trough advanced eastward, although the maximum height at 850 hPa was centered over the Isthmus of Tehuantepec and Guatemala (not shown). At this time (14/12), the largest separation between the surface and 850-hPa anticyclone occurred (over 1600 km) and may be attributed to the modification of the cold anticyclone over the Gulf of Mexico. The warm waters of the gulf heat and moisten the air column, thereby reducing the pressure of the anticyclone in the lowest layers of the atmosphere (e.g., Colle and Mass 1995), while 850 hPa remains relatively unaffected. Thus, the highest surface pressure remained over the land surface, but the center of the 850-hPa anticyclone moved farther south, channeled by the mountains.

The leading edge of the cold air at the surface passed Belize and progressed equatorward into Honduras at 13/12 (Fig. 3d), into Costa Rica at 14/00 (Fig. 5a), and into Panama by 14/12 (Fig. 6a). At 13/12, the leading edge of the surge was characterized by a strong surface potential temperature gradient [$\sim$6°C $(200\ km)^{-1}$] followed by a broader region of weaker potential temperature gradient [$\sim$6°C $(600\ km)^{-1}$] (Fig. 3d). But by 14/00, the surface potential temperature gradient at the leading edge had weakened considerably, whereas the leading edge of the cold air at 850 hPa was about 200 km farther south than at the surface. Mesoscale ridging occurred along the east side of the mountain chain in Honduras and Nicaragua at 14/00 (Fig. 5a). The impact of the surge was to increase the cloudiness in the Gulf of Mexico and surrounding land area as illustrated by the high relative humidity in the lower troposphere (Fig. 5d). In addition to ascent along the east side of the Sierra

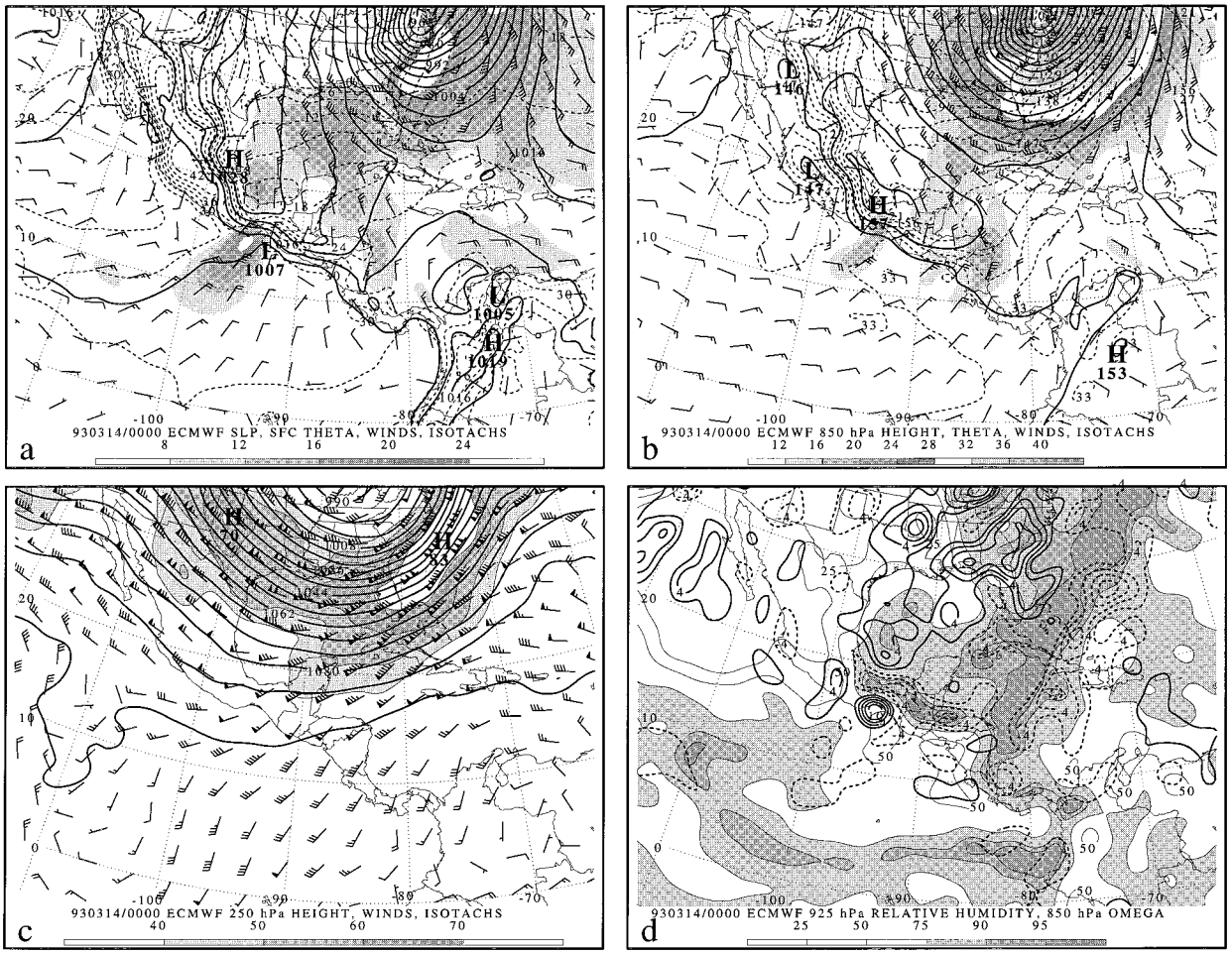

FIG. 5. ECMWF analyses at 0000 UTC 14 March 1993. (a) Sea level pressure (solid lines every 4 hPa), surface potential temperature (dashed lines every 3°C), 10-m wind (one pennant, full barb, and half-barb denote 25, 5, and 2.5 m s^{-1}, respectively), and wind speed (m s^{-1}, shaded). (b) The 850-hPa geopotential height (solid lines every 3 dam), 850-hPa potential temperature (dashed lines every 3°C), 850-hPa wind [as in (a)], and wind speed (m s^{-1}, shaded). (c) The 250-hPa geopotential height (solid lines every 6 dam), 250-hPa wind [as in (a)], and wind speed (m s^{-1}, shaded). (d) The 925-hPa relative humidity (shaded and contoured as noted by scale on bottom of panel) and 850-hPa vertical velocity [every 0.2 Pa s^{-1}, thick solid lines (thick dashed lines) represent descending (ascending) motion].

Madre mountains from Veracruz, Mexico, to Costa Rica, the strongest localized descent on the west side occurred in the lee of the Isthmus of Tehuantepec (Fig. 5d). Also, the 925-hPa relative humidity analysis shows the extensive moist area confined behind the norther where the flow was ascending the mountains. Another band of ascent associated with the cold-frontal zone extended from Costa Rica poleward to off the east coast of the United States. The strength of the northerlies over Panama increased despite the CACS still being over 300 km away (cf. Figs. 3a,b with Figs. 5a,b); the reason for this increase is unclear.

By 14/00, the leading edge of the cold surge had advanced equatorward underneath the 250-hPa jet entrance region (Fig. 5c), suggestive of a coupled circulation (e.g., Lau and Chang 1987) between the direct upper-level circulation associated with the jet entrance region (e.g., Beebe and Bates 1955; Uccellini and Johnson 1979) and the direct frontal circulation associated with the cold surge. To diagnose these two circulations, the psi-vector methodology of Loughe et al. (1995) for partitioning divergent ageostrophic circulations into orthogonal cross sections is employed. Since the geostrophic wind on an *f* plane (in this case, centered at 25°N) is nondivergent, the total divergence is therefore associated with the ageostrophic wind.

Figure 7 illustrates the divergent ageostrophic wind and the corresponding velocity potential at 850 hPa and 250 hPa for 12/12 and 13/12. At 12/12, a nearly circular region of 850-hPa convergence occurred over the cyclone center associated with 250-hPa divergence aloft (Figs. 7a,b).[4] By 13/12, the 850-hPa convergence as-

[4] The Laplacian of the velocity potential is proportional to the divergence [e.g., Loughe et al. 1995, their Eq. (2.11)].

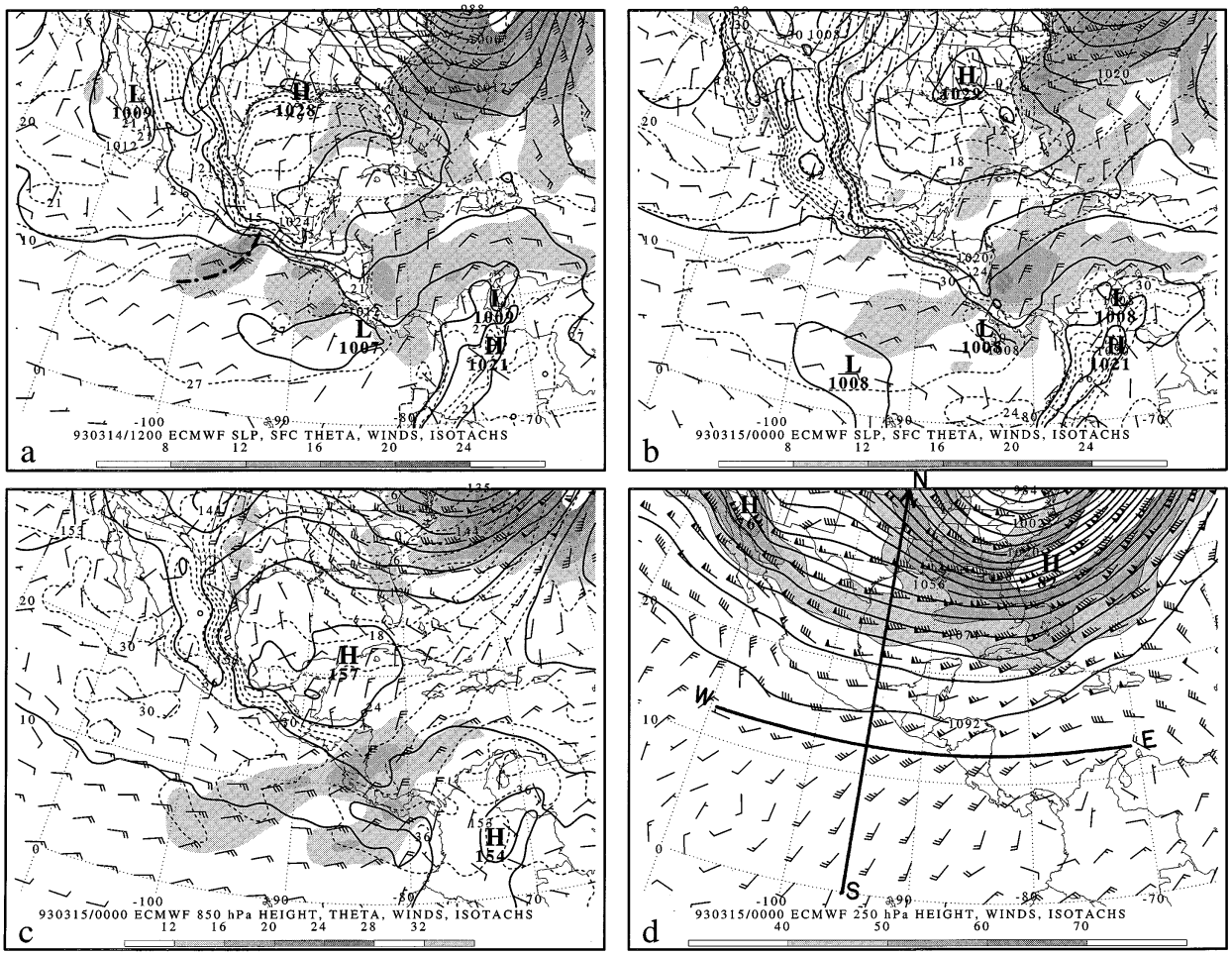

FIG. 6. ECMWF analyses. (a) The 1200 UTC 14 March 1993 sea level pressure (solid lines every 4 hPa), surface potential temperature (dashed lines every 3°C), 10-m wind (one pennant, full barb, and half-barb denote 25, 5, and 2.5 m s^{-1}, respectively), and wind speed (m s^{-1}, shaded). (b) Same as (a) except for 0000 UTC 15 March 1993. (c) The 0000 UTC 15 March 1993 850-hPa geopotential height (solid lines every 3 dam), 850-hPa potential temperature (dashed lines every 3°C), 850-hPa wind [as in (a)], and wind speed (m s^{-1}, shaded). (d) The 0000 UTC 15 March 1993 250-hPa geopotential height (solid lines every 6 dam), 250-hPa winds [as in (a)], and wind speed (m s^{-1}, shaded). The location of cross section south–north (SN) from Fig. 4b and cross section west–east (WE) from Fig. 4c identified by thick solid lines. Dash–dot line in (a) represents a trajectory of an air parcel in an inertial circle with an initial wind speed of 20 m s^{-1} and a radius of 530 km.

sociated with the low-center had strengthened and moved northeast as a band of convergence extended southwestward from the low center and was oriented along the leading edge of the cold surge. The familiar four-cell pattern of upper-level divergence/convergence associated with a straight jet streak may be masked in these calculations by the contribution from the cyclonic curvature of the large-scale trough (e.g., Moore and VanKnowe 1992).

To separate the ECMWF omega field into the contribution from the frontal-scale circulation at the leading edge of the cold surge and that attributed to the confluent jet entrance region aloft, a cross section normal to the low-level surge is selected. Cross section *AB* lies roughly parallel to the terrain of Mexico and Central America, nearly normal to the orientation of the leading edge of the surge, but away from the topography (Fig. 7). Therefore, divergent circulations within the plane of the cross section can be thought of as the frontal-scale component, whereas circulations normal to the plane of the cross section can be thought of as the synoptic-scale component associated with the baroclinic disturbance aloft. Because *AB* does not lie normal to the long axis of the jet, particularly at 13/12, this partition is not exact; nevertheless, these results will be of qualitative value.

At 12/12, the divergent circulation in the plane of *AB* was much stronger and possessed more mesoscale structure than that normal to *AB* (cf. Figs. 8a,b). A tropospheric-deep direct circulation linked the leading edge of the cold surge to the jet entrance region aloft (Fig. 8a). By 13/12, the surge and its accompanying vertical circulation were still linked to the jet aloft and had pro-

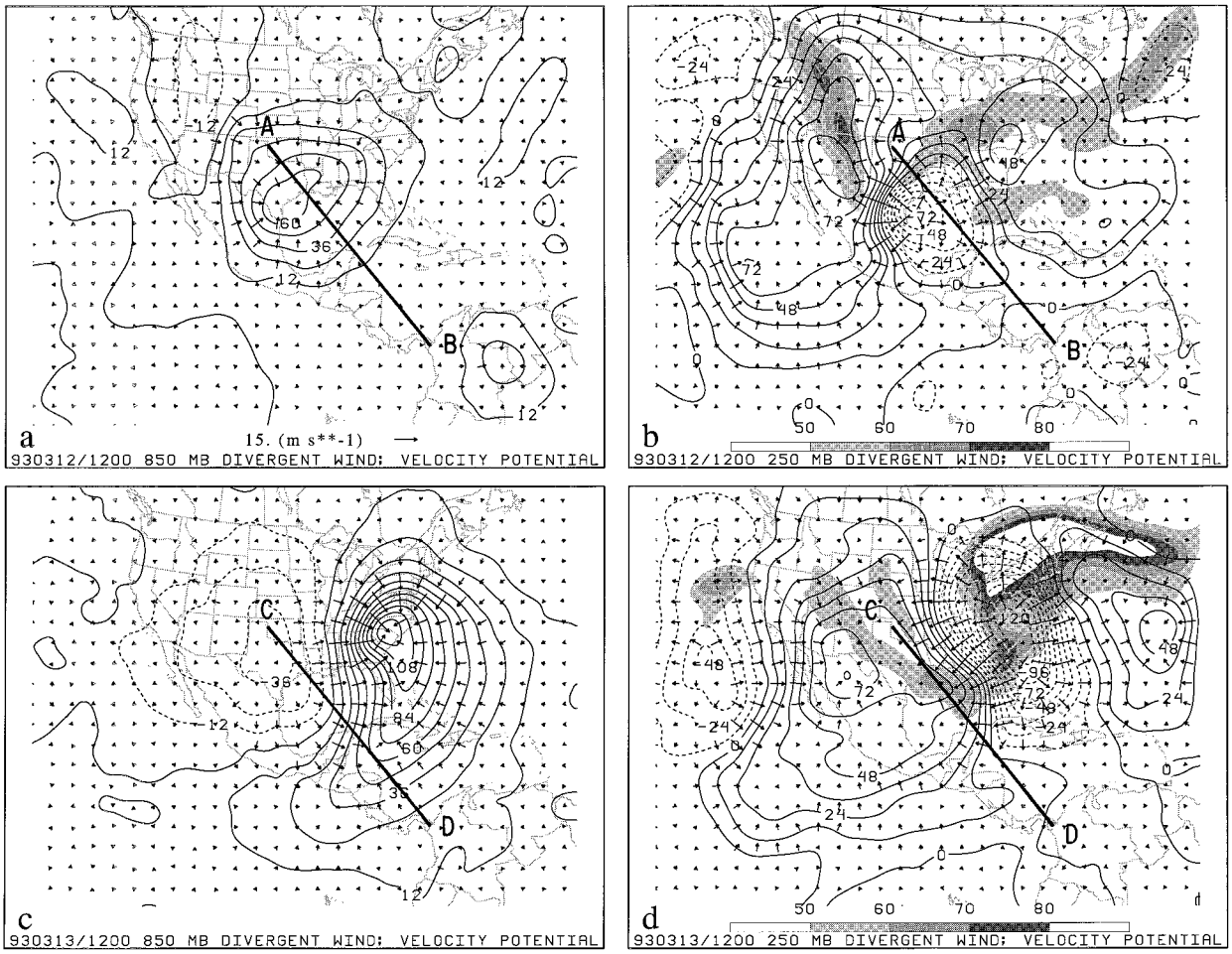

FIG. 7. Divergent wind (m s^{-1}) and velocity potential (every 12×10^5 m^2 s^{-1}). Cross sections in Fig. 8 indicated by heavy lines labeled *AB* and *CD*. Isotachs of total 250-hPa wind in (b) and (d) (m s^{-1}, shaded). (a) 1200 UTC 12 March 1993 850 hPa. (b) 1200 UTC 12 March 1993 250 hPa. (c) 1200 UTC 13 March 1993 850 hPa. (d) 1200 UTC 13 March 1993 250 hPa.

gressed equatorward (Fig. 8c). Strong northerlies behind the surge were associated with the deep frontal-scale circulation and the strong descent behind. The circulation normal to *AB* (Fig. 8d) indicated a broad region of subsidence behind the cold surge, likely associated with the descent on the west side of the upper-level trough over the Gulf of Mexico (Fig. 3c), maintaining the lower-tropospheric anticyclone. Therefore, at this time, the deep frontal-scale circulation at the leading edge of the surge with the northerlies behind (Fig. 8c), associated with the broad region of descent in the cold air (Fig. 8d) maintaining the anticyclone, were indicative of a coupled circulation between the upper-level jet entrance circulation and the lower-level frontal circulation. By 14/12 (not shown), the leading edge of the cold surge had advanced farther equatorward and the jet entrance region had moved eastward, thereby decoupling the two circulations; further equatorward advance of the surge was minimal.

Returning to the horizontal maps, the strong pressure gradient along the Sierra Madre in Mexico and resulting downslope flow produced a lee trough south of Baja California at 13/12 (Fig. 3d). Another effect of the equatorward advance of the anticyclone was to create a pressure difference of over 12 hPa across the Isthmus of Tehuantepec (Fig. 3d). Forced to accelerate down the pressure gradient within Chivela Pass, surface winds then traveled over the Gulf of Tehuantepec, attaining speeds greater than 20 m s^{-1}. Note that the strongest winds occur over the Gulf of Tehuantepec downstream from the gap and not in the narrowest part of the gap, consistent with gap flow in the Strait of Gibraltar (Dorman et al. 1995). Dorman et al. (1995) hypothesized that the presence of a lower-tropospheric inversion aided in the flow acceleration through the gap; the stable layer above the Isthmus of Tehuantepec at about 800 hPa (e.g., Fig. 4a) may play a similar role. There is also a suggestion of 1°–3°C cooling of the surface potential temperature over the Gulf of Tehuantepec (cf. Figs. 2d and 3d).

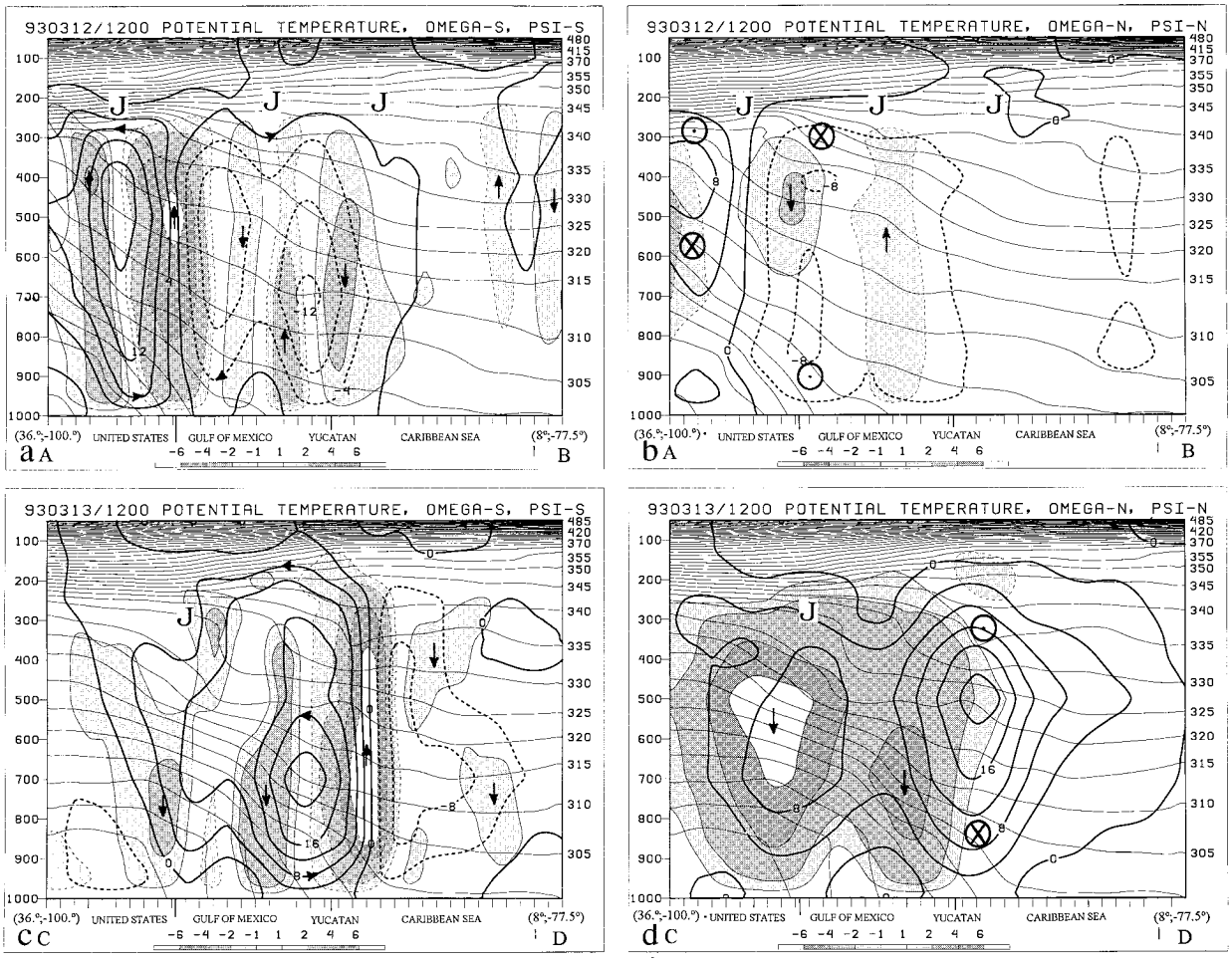

FIG. 8. Cross sections *AB* and *CD* from Fig. 7. Potential temperature (thin solid lines every 5 K). Here, ''J'' represents location of total wind maximum. Arrows indicate direction of circulation. (a) Streamfunction for divergent circulation (thick solid lines every 4×10^4 Pa m s^{-1}) and omega (0.1 Pa s^{-1}, shaded) in the plane of *AB* at 1200 UTC 12 March 1993. (b) Streamfunction for divergent circulation (thick solid lines every 4×10^4 Pa m s^{-1}) and omega (0.1 Pa s^{-1}, shaded) normal to *AB* at 1200 UTC 12 March 1993. Circle surrounding dot (X) represents flow out of (into) page. (c) Same as (a) except for 1200 UTC 13 March 1993 along cross section *CD*. (d) Same as (b) except for 1200 UTC 13 March 1993 along cross section *CD*.

Twelve hours later at 14/00, the tehuantepecer attained its maximum intensity of 25 m s^{-1}, forced by a cross-isthmus sea level pressure difference of over 16 hPa (Fig. 5a). By 14/12, the tehuantepecer weakened to under 20 m s^{-1} as the cross-isthmus pressure difference had decreased to about 12 hPa (Fig. 6a). In time, the strongest winds associated with the tehuantepecer began to expand and rotate clockwise (cf. Figs. 3d and 6a). The rotation of the tehuantepecer winds from nearly northerly to northeasterly is consistent with the expected Coriolis deflection of an inertial jet discussed by Clarke (1988), who noted the similarity between the shape of the upwelled water in the Gulf of Tehuantepec and an inertial circle. At 15°N for a 20 m s^{-1} wind, the radius of an inertial circle is about 530 km (e.g., Holton 1992, 64–65). The arc of a circle with a radius of 530 km originating at the Gulf of Tehuantepec is very similar to the region of maximum winds (Fig. 6a). The equatorward portion of the region of maximum wind speed also had a smaller inertial radius of curvature, consistent with the weaker wind speed away from the gap.

While the tehuantepecer winds were decreasing at 14/12, surface winds of greater than 12 m s^{-1} had appeared in the Gulfs of Fonseca, Papagayo, and Panama in response to the surge of higher pressure on the east side of Central America (Fig. 6a). The northerly wind over Panama appears to have resulted from a merger of the persistent northeasterlies north of Venezuela and the northerlies associated with the CACS.

Ahead of the cold surge, the easterly flow north of South America veered poleward ahead of SS93 as the inverted trough north of Panama and the trough south of SS93 met, weakening the sea level pressure gradient over the Caribbean Sea southwest of Jamaica (Fig. 3d).

Riehl (1954, p. 270) noted that inverted troughs often precede cold surges into the Tropics. Pressure increases behind the surge over the Caribbean also caused the lower-tropospheric winds in this area to come from the north-northeast by 14/12 (Fig. 6a). Finally, the effect of the norther on the tropical circulation became evident as the lower-tropospheric northeasterly trade winds near the region (5°N, 95°W) began strengthening (Figs. 6b,c).

Therefore the major characteristics of the mature stage of the cold surge included a 16-hPa pressure gradient across the isthmus and the resulting gap flow down the pressure gradient, which produced a tehuantepecer, the anticyclonic rotation of the axis of maximum wind associated with the tehuantepecer, the development of gap winds in the Gulfs of Fonseca, Papagayo, and Panama, and the movement of the surge underneath the confluence aloft implicating a coupled circulation between the direct secondary circulations associated with the upper-level jet entrance region and the low-level frontal zone.

c. Decay of the cold surge: 0000 UTC 15 March–0000 UTC 16 March 1993

At 15/00, the Caribbean Sea was covered by cool air in the lower troposphere associated with the CACS (Fig. 6c). Strong potential temperature gradients at the surface and 850 hPa were apparent along the eastern slope of the Sierra Madre even as the main baroclinic region continued to advance toward the south and east across the Caribbean and western Atlantic (Figs. 6c,d). Also over the northern Gulf of Mexico, 10 m s^{-1} winds were directed down a relatively weak sea level pressure gradient (Fig. 6b). The reason for the magnitude of this ageostrophy is unclear. Winds in the topographic gaps (Tehuantepec, Fonseca, Papagayo, and Panama) had all decreased; however, the areal extent of the winds in the Gulfs of Panama and Papagayo expanded and turned clockwise (Figs. 6b,c).

Figure 4b, a vertical cross section at 15/00 along the same north–south line as Fig. 4a, shows the pooling of the cold air on the windward side of the isthmus. The cold surge remained connected to the main cold-air reservoir in the United States while both the separation between the two features and the lower- and midtropospheric stability within the polar air over the southern United States had increased (cf. Figs. 4a,b). By this time the northerlies in the lower troposphere over the Gulf of Tehuantepec were found only within approximately 300 km of the isthmus. Farther equatorward, the northeast trade winds appeared to have become better organized and more intense during this period (cf. Figs. 4a,b). An east–west cross section along 12.5°N at 15/00 (Fig. 4c) shows that the northerlies and the cool air remained anchored to the east slopes of the topography, illustrating the similarity of the topographically trapped cold surge to cold-air damming events (e.g., Bell and Bosart 1988; Colle and Mass 1995). Note that the cold dome extends higher than the topography and farther eastward than the Rossby radius L_R of about 100 km [$L_R = Nh/f$, where the buoyancy frequency $N \sim 3.5 \times 10^{-3}$ s^{-1}, the mountain height $h \sim 1000$ m, and $f(12.5°N) = 3.2 \times 10^{-5}$ s^{-1}], suggesting that topographic effects alone cannot explain the structure of the surge—dynamic forcing due to the low-latitude upper-level trough and confluent jet entrance region circulations may also contribute to the structure of the cold pool (e.g., Figs. 7 and 8).

At 15/12, as the surface anticyclone moved to the northeast (Fig. 9a), it was replaced by a developing cyclone in the lee of the southern Rockies, apparently in response to an advancing short-wave trough in the westerlies over northern Mexico (Figs. 6d and 9d) inducing southerly flow over the Central Plains of the United States and the east coast of Mexico. The lower-tropospheric ascent–descent dipole over Central America was at its farthest equatorward extent (not shown), and the low-level wind speed in the Gulf of Panama increased slightly (Fig. 9a).

Finally by 16/00, the tehuantepecer dissipated with the loss of most of the pressure difference across the isthmus (Fig. 9b). At this time, there was a continued strengthening of the northeast trade winds in the eastern Pacific Ocean (Figs. 9b,c) and a reduction in the strength and areal extent of the cross-equatorial flow at 250 hPa (Fig. 9d). At the surface, a band of surface convergence along 5°N over the eastern Pacific was bounded by southerly cross-equatorial flow and the strengthened northeast trades (Fig. 9b) favoring a band of ascent in the lower troposphere (not shown). This may indicate that the cold surge led to enhanced trade winds, increased surface convergence, and an increase in convection along the ITCZ (see section 1b), the same effect observed in conjunction with East Asian cold surges (e.g., Chang et al. 1979).

d. Summary

The salient features of the large-scale aspects of the CACS associated with SS93 are summarized below. An anticyclone from Alaska and western Canada expanded into the central United States and was the source of the cold air for the surge into Central America. The surge was initiated in the wake of a developing cyclone in the lee of the Sierra Madre, apparently associated with an advancing upper-level short-wave trough. A situation similar to cold-air damming resulted in terrain-parallel flow, which caused the surge to advance equatorward. Cross sections through the cold surge demonstrate that it was tied to the synoptic-scale baroclinic zone associated with the upper-tropospheric jet stream. As the surge advanced equatorward, the separation between the jet and the leading edge of the surge increased and the lower and midtropospheric stability within the polar air increased. The unusual strength and equatorward extent of the cold surge suggest a coupling between orographic

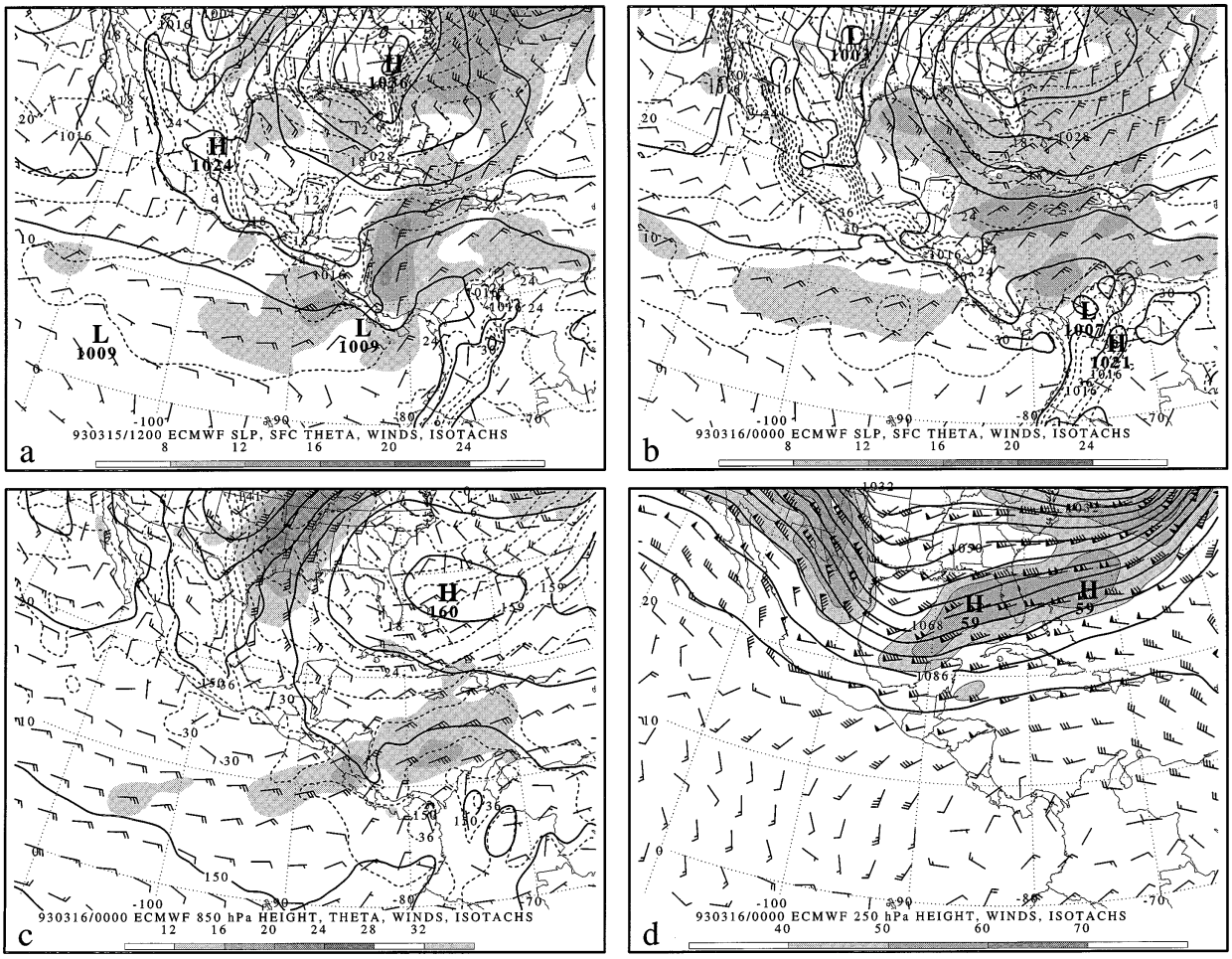

FIG. 9. Same as for Fig. 6 except for 1200 UTC 15 March 1993 in (a) and 0000 UTC 16 March 1993 in (b), (c), and (d).

and synoptic-dynamic effects. An upper-tropospheric confluent jet entrance region over Mexico/Central America favored a direct secondary circulation east of the mountains, aiding the strength and equatorward movement of the cold surge. This is also indicated by the separation of the surface anticyclone into two pieces, one moved with the synoptic flow over the southeast United States and the other moved equatorward along the mountains behind the leading edge of the surge.

In the Gulfs of Tehuantepec, Fonseca, Papagayo, and Panama, 10–25 m s^{-1} gap winds were observed. These appear to be related to the strong sea level pressure gradients across the topography. In time, the gap-wind events over the eastern Pacific Ocean turned anticyclonically, likely because of the Coriolis torque (Clarke 1988). The northeast trades increased in strength as the gap winds moved over the tropical Pacific Ocean. The tehuantepecer weakened after the center of the 850-hPa anticyclone moved equatorward of the Isthmus of Tehuantepec along the Central American mountains and the 850-hPa cross-mountain pressure gradient decreased.

5. Mesoscale analysis

In this section the observational data are used to examine the structure and evolution of the CACS associated with SS93. Figure 10 summarizes the isochrones of the rope clouds associated with the leading edge of the cold surge from 12/14 to 14/06 as determined from the available visible and infrared satellite imagery. The rope clouds can be interpreted in the discussion that follows as localized regions of surface convergence and are correlated with weather changes from the surface observations. Five different cloud bands (numbered 1–5) were identified during this period and are discussed in detail below.

a. Initiation of the cold surge: 1200 UTC 12 March–0000 UTC 13 March 1993

At McAllen, Texas (MFE), a classic frontal passage (e.g., Sanders 1955) with a near-simultaneous pressure minimum and southeast to northwest wind shift, was

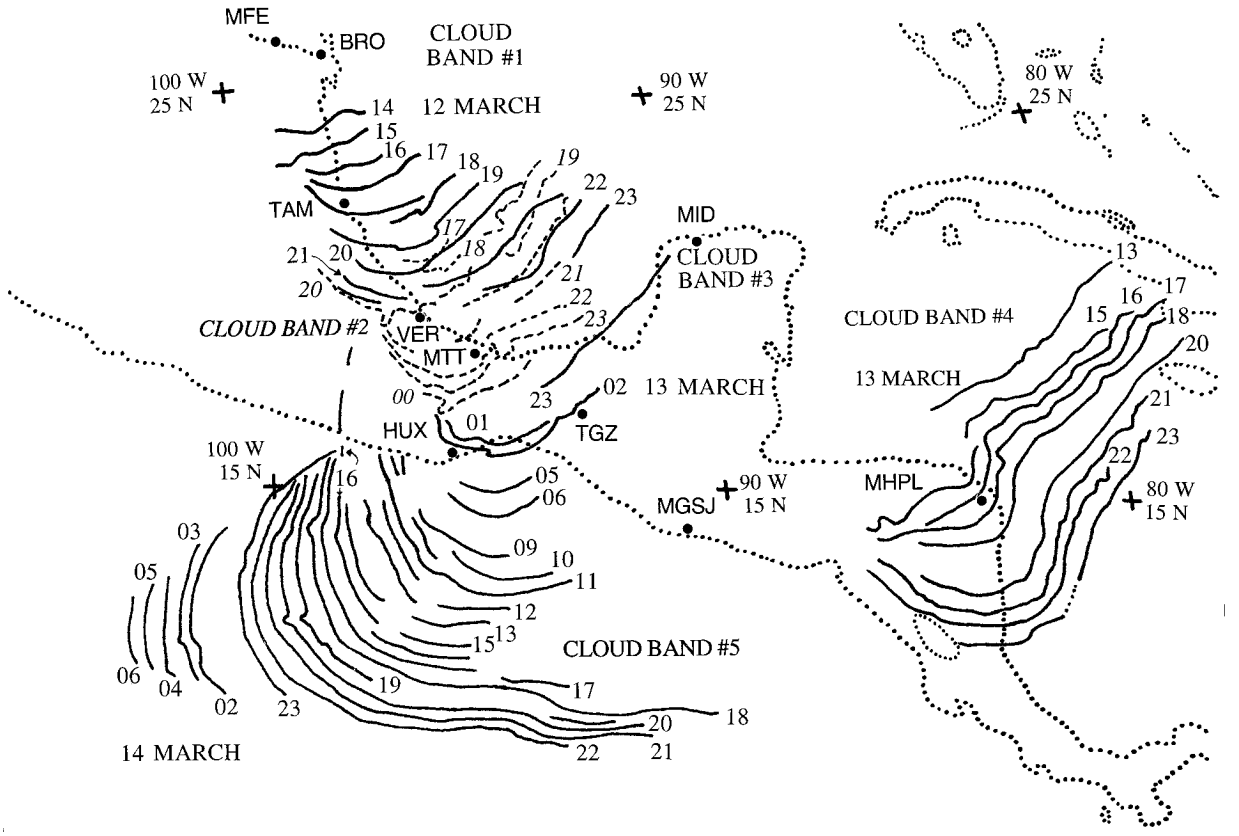

FIG. 10. Isochrones of cloud bands as determined from available visible and infrared satellite imagery. All cloud bands drawn in solid lines unless otherwise noted. Dates and times (UTC) labeled in normal typeface unless otherwise noted. Dash–dot line represents a trajectory of an air parcel in an inertial circle with an initial wind speed of 20 m s^{-1} and a radius of 530 km. Cloud band 1: 1400 UTC–2300 UTC 12 March. Cloud band 2: 1700 UTC 12 March–0000 UTC 13 March (dashed lines, italics). Cloud band 3: 2300 UTC 12 March. Cloud band 4: 1300 UTC–2300 UTC 13 March. Cloud band 5: 0100 UTC 13 March–0600 UTC 14 March.

observed at 1058 UTC 12 March; the following hour, the temperature and dewpoint fell 4.4°C and 7°C, respectively (Fig. 11a). Farther east at BRO, a trough passed at 1025 UTC followed by a wind shift from southeast to west (not shown). At 1204 UTC, heavy thundershowers and pea-sized hail coincided with a sustained west wind of 19 m s^{-1}. After rapid (~15–30 min) pressure fluctuations, apparently associated with the convection, subsided (confirmed from the BRO barogram, not shown), the pressure began to rise steadily as the wind weakened and veered to northwest, before strengthening again as the cold air arrived. Therefore, we suspect that these pressure and wind fluctuations at BRO, obscured an otherwise classic cold-frontal passage, as occurred at MFE.

The leading edge of the cold surge, indicated by a rope cloud in visible satellite imagery, was first clearly identified at 1401 UTC in northern Mexico (Fig. 10). A visible satellite image 2 h later (1601 UTC, Fig. 12a) shows SS93 developing in the western Gulf of Mexico and the rope cloud (hereafter cloud band 1) emerging from the southwestern portion of the cloud mass.

The hourly observations from Tampico, Mexico (TAM), indicate a minimum altimeter setting of 1003.4 hPa at 1145 UTC 12 March (not shown). The next available observation at 1545 UTC reported an altimeter setting 2.0 hPa higher and weak (3 m s^{-1}) south-southwesterly winds. At 1735 UTC, 6 m s^{-1} northerlies gusting to 10 m s^{-1} arrived at TAM, coincident with a 2.0-hPa increase in the altimeter setting and a 2°C temperature drop. Except for the pressure rise before the frontal passage, the temperature and dewpoint decreases occurred simultaneously with the wind shift. The presurge pressure increase, however, had the opposite tendency to the diurnal pressure cycle.

Around this time (12/18), low cloud elements parallel to and ahead of cloud band 1 organized to form cloud band 2 (Fig. 10). Figure 12b illustrates the formation of the second cloud band at 1801 UTC south of TAM (possibly indicating why this cloud band was not reflected in the surface observations at TAM). A surface map from this time (Fig. 13) indicates that the cold surge was moving toward VER. The along-terrain sea level pressure gradient extended over 1000 km poleward from the surface cold front to northern Texas, providing a long region for topographically trapped flow and confining the cold

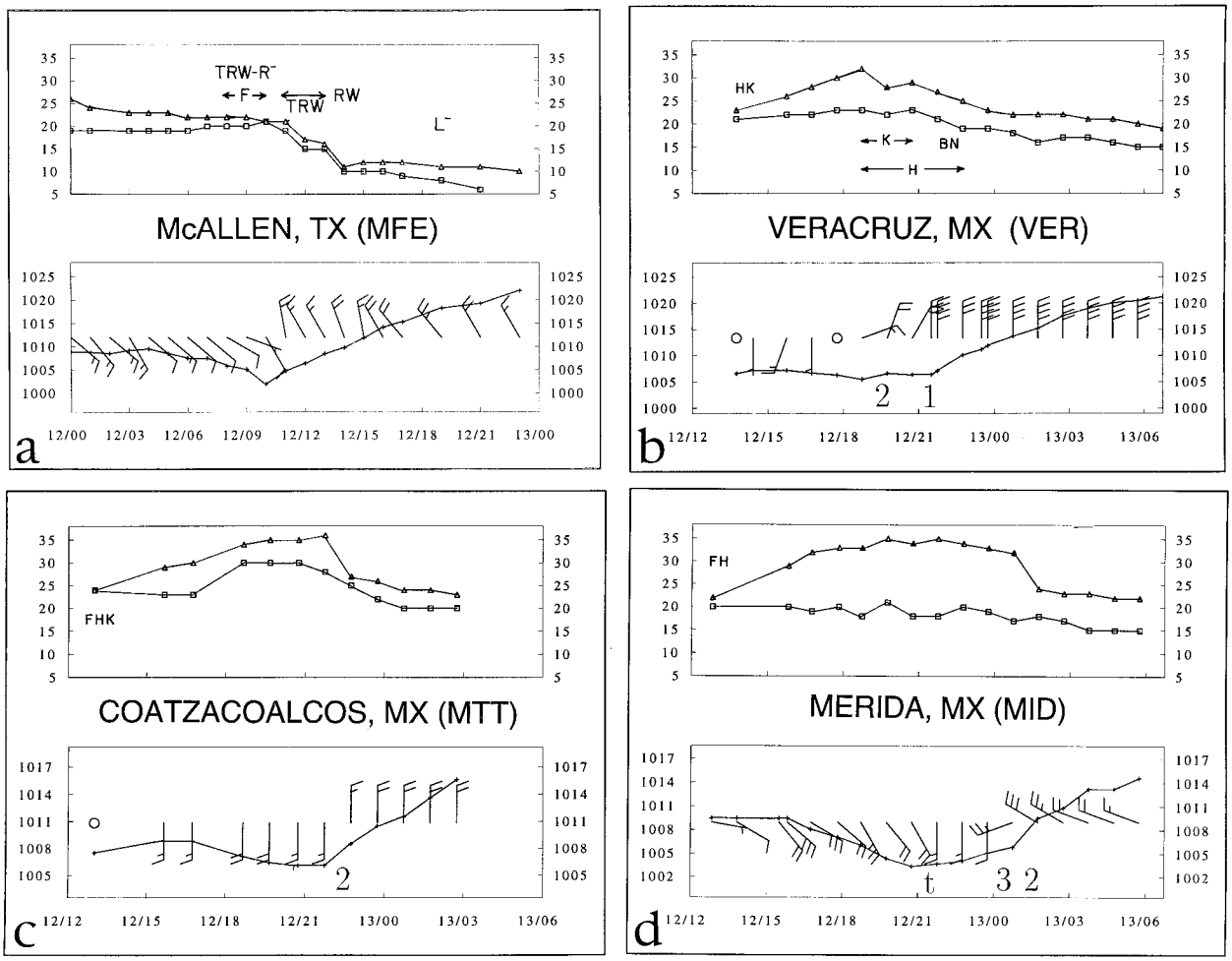

FIG. 11. Meteorograms. Top: temperature (°C, triangles), dewpoint (°C, squares) and significant weather. T = thunderstorms, R = rain, W = showers, A = hail, H = haze, K = smoke, BN = blowing sand, F = fog, L = drizzle, + = heavy, and − = light. Bottom: sea level pressure (hPa) and wind (one pennant, full barb, and half-barb denote 25, 5, and 2.5 m s^{-1}, respectively). Numbers 1–4 represent passage of cloud bands; t = trough passage. (a) McAllen, Texas (MFE); (b) Veracruz, Mexico (VER, 76691); (c) Coatzacoalcos, Mexico (MTT, 76741); (d) Merida, Mexico (MID, 76644); (e) Puerto Lempira, Honduras (MHPL, 78711); (f) Bahias de Huatulco, Mexico (HUX); (g) Tuxtla Gutierre, Mexico (TGZ, 76843); and (h) San Jose, Guatemala (MGSJ, 78647).

air to the east side of the Sierra Madre. In advance of the cold surge, a trough, indicated by a wind shift from south-southeast to southwest, extended equatorward from the center of SS93 (this same trough can be seen in the ECMWF analysis at 13/00 in Fig. 3a). This trough may represent the remnants of an airmass boundary between moist Gulf of Mexico air and dry Mexican air that was transported offshore and served as the focal point for development of the squall line that devastated portions of Florida and Cuba on 13 March.

At 12/20, cloud band 2 passed VER and the winds turned northeasterly at 10 m s^{-1} as the pressure rose 1.1 hPa and then leveled off (Fig. 11b). Although an afternoon sea-breeze flow from the east-northeast usually affects VER and cannot be entirely discounted in this case, the simultaneous arrival of cloud band 2 as the winds freshen out of the northeast suggests that the wind shift was related to the passage of the cloud band. The remnants of cloud band 1, moving at an average speed of 20 m s^{-1}, passed VER at 2130 UTC when the winds shifted to northerly at 15 m s^{-1}, gusting to 20 m s^{-1}, and the pressure began rising 2–3 hPa h^{-1}. Fifteen minutes later, the northerly winds at VER increased to 20 m s^{-1}, gusting to 33 m s^{-1}. At 12/21, the leading edge of the cold surge still was associated with cloud band 1.

Figure 12c shows cloud band 2, moving at an average speed of about 15 m s^{-1}, entering the Isthmus of Tehuantepec at 2201 UTC. The farther advance of the cloud band near the mountains compared to over the Bay of Campeché illustrates the acceleration of the cold surge adjacent to the topography in this region (Figs. 10 and 12c). Also at this time a new cloud band (cloud band 3) appeared to be organizing just west of the Yucatán Peninsula as cloud band 1 dissipated (Figs. 10 and 12c). Coatzacoalcos, Mexico (MTT) (formerly Puerto Mexico) experienced a classic cold-frontal passage ac-

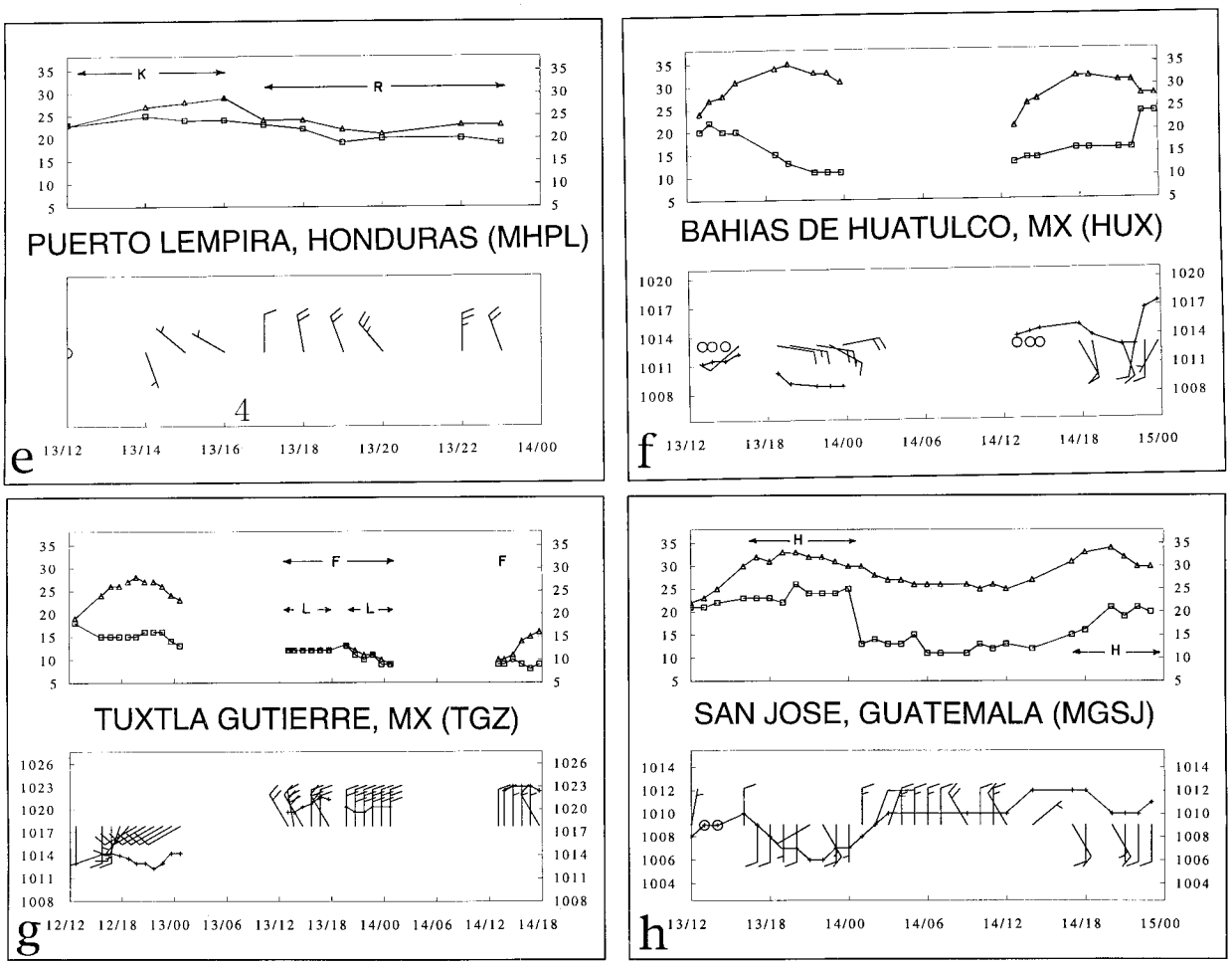

FIG. 11. (*Continued*)

companied by a large pressure rise, a temperature drop of 9°C from 36°C in 1 h, and a wind shift from south to north as cloud band 2 passed between 2145 and 2245 UTC (Fig. 11c). Cloud band 3 formed to the east of MTT, and cloud band 1 did not appear to ever reach MTT. Therefore, by the time the cold surge had reached MTT, cloud band 2 had appeared to become the leading edge of the cold surge.

The minimum pressure at Merida, Mexico, was attained at 2045 UTC 12 March (Fig. 11d). A subtle wind shift from southeast to south accompanied this pressure rise, which appears to be related to the passage of the trough to the south of the surface cyclone (Fig. 13). The pressure rose slightly and the wind shifted from southerly to southwesterly at 13 m s^{-1} with little temperature change as cloud band 3 passed MID between 12/23 and 13/01 (Fig. 11d). During the next hour, the leading edge of the cold surge passed MID, dropping the temperature by 8°C and causing the wind to veer to the northwest. It seems likely that the remnants of cloud band 2 (unable to be tracked owing to the lack of nighttime visible imagery), and still apparently the primary surge, passed MID at this time.

From the surface observations and satellite imagery, the following evolution appears evident. The cold surge initially began as a classic cold front with the pressure minimum and shift to northerly wind component nearly coincident; the sharp temperature decrease arrived shortly thereafter. Eventually a pressure minimum developed out ahead of, or outran, the leading edge of the strong northerlies (unable to distinguish owing to data limitations). Cloud elements organized within this presurge pressure minimum, eventually developing a rope cloud (hereafter called *the presurge cloud band*). The winds also increased in speed and in northerly component between the leading edge of the surge and the presurge cloud band. The primary surge and its accompanying cloud band appeared to last on the order of 6–10 h before being supplanted by the presurge cloud band as the warm air between the main surge and the presurge cloud band apparently became progressively diluted by cooler, higher momentum northerlies. Eventually, the air in this

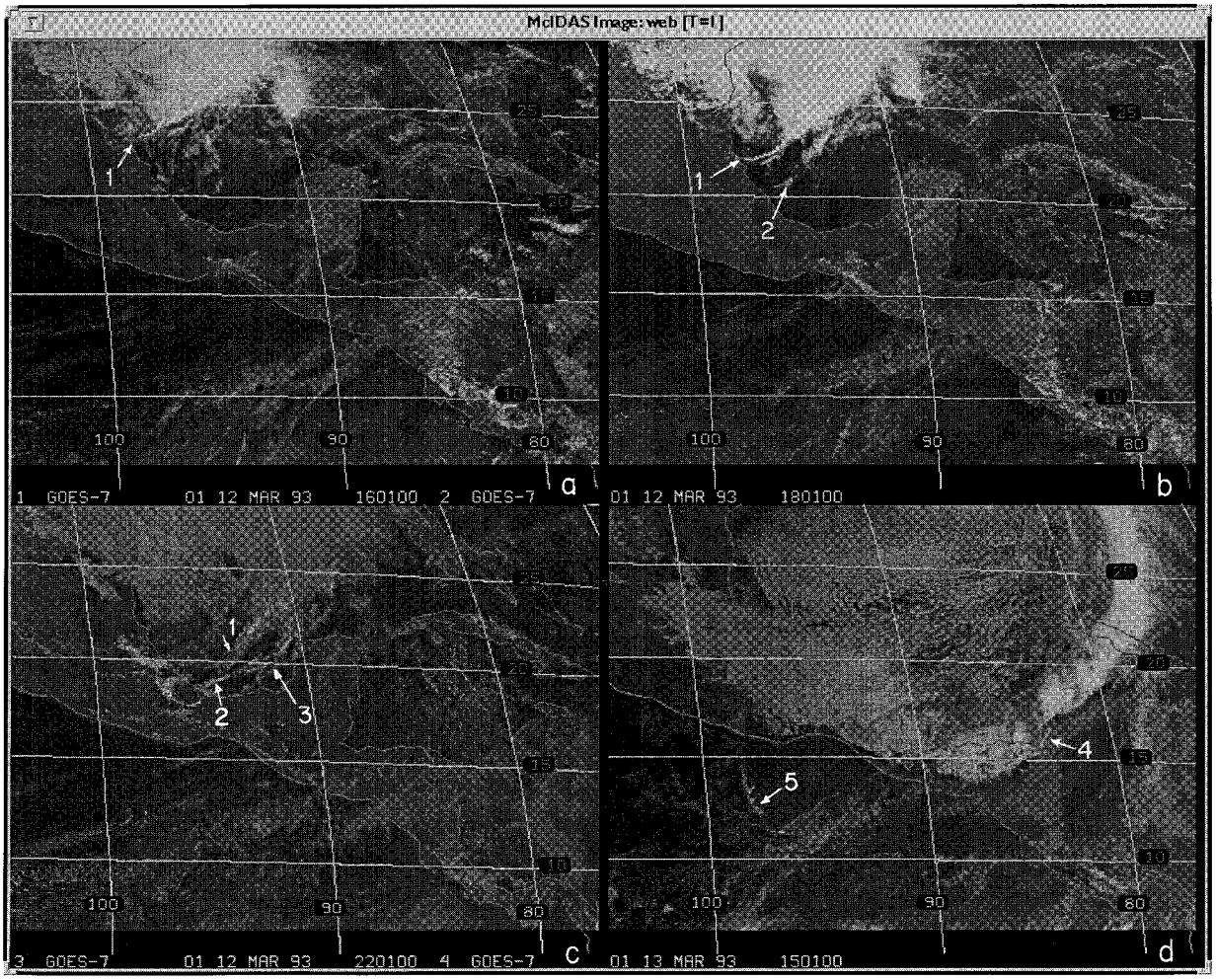

FIG. 12. *GOES-7* visible satellite imagery. Numbers represent cloud bands 1–5: (a) 1601 UTC 12 March, (b) 1801 UTC 12 March, (c) 2201 UTC 12 March, (d) 1501 UTC 13 March, and (e) 1801 UTC 14 March.

transition zone became so diluted with the cooler air that the presurge cloud band became the leading edge of the cool air. Further discussion of the nature of this evolution follows in section 6b.

b. Maturation and decay of the cold surge: 1200 UTC 13 March–1200 UTC 16 March 1993

The return of visible satellite imagery by 13/15 (Fig. 12d) shows two rope clouds, one extending from the comma cloud associated with SS93, equatorward across Cuba and eastern Honduras (cloud band 4), and the other emanating south and west from the Isthmus of Tehuantepec (cloud band 5). Cloud band 5 resembles the arc-shaped cloud associated with a tehuantepecer discussed by Hurd (1929) and Parmenter (1970). Because of the loss of visible imagery during the night, it is difficult to trace the evolution of cloud band 3 into cloud band 4 and also to determine whether cloud band 5 was a continuation of cloud band 2 or a newly formed cloud band. As a result, we identified these rope clouds as new features, although there was no way to determine their origin conclusively from the available satellite imagery.

As cloud band 4 encountered the bend in the Central American coastline in northern Nicaragua (Fig. 1), the surge accelerated near the coast, producing first a break (Fig. 12d) and later a bend in the rope cloud (Fig. 14a). As the surface anticyclone expanded into lower latitudes, the isobars became zonally oriented along similarly oriented topography in western Honduras. When the leading edge of the surge passed the eastward edge of the mountains near Puerto Lempira, Honduras (MHPL), the flow accelerated down the still meridionally oriented pressure gradient. This imbalance thereby effected a temporary acceleration of the surge near the coastline and a bend in cloud band 4 (as discussed for idealized simulations by Skamarock et al. 1996). In addition, weakly organized, linear cloud bands appeared to be present in the presurge environment over eastern

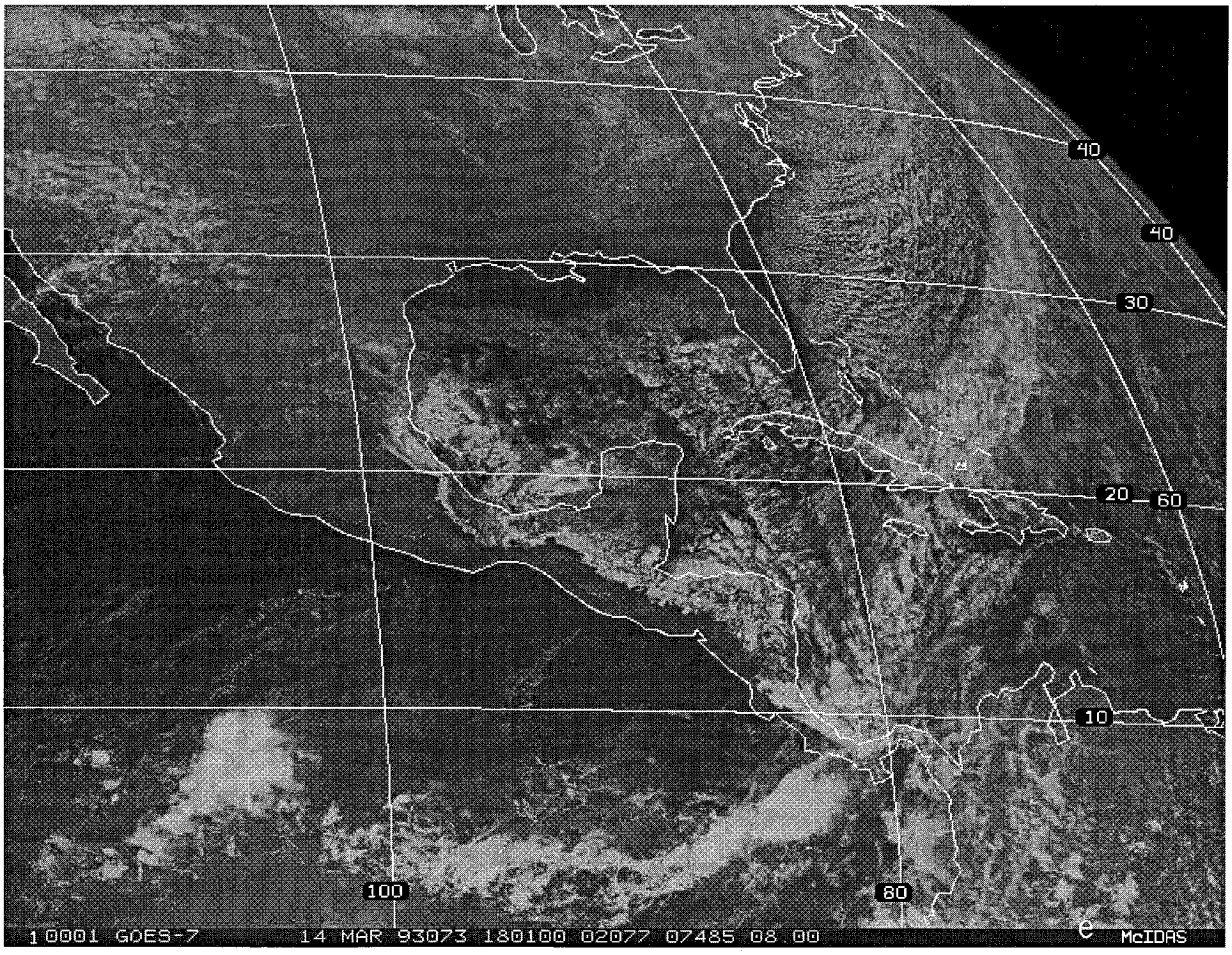

FIG. 12. (*Continued*)

Nicaragua (Figs. 12d and 14a), reminiscent of the pre-surge cloud bands along the Mexican coast. Due to the absence of surface observations over Nicaragua, the weak organization of these cloud bands, and the difficulty in determining their movement, we have not attempted to systematically track them.

Frontal passage at MHPL occurred between 1600 and 1700 UTC when the temperature dropped 5°C and rain replaced smoke as the significant weather—weather indicative of an atemporalado (Fig. 11e). This time is coincident with the passage of cloud band 4 as determined from the satellite imagery (Fig. 10). Figure 14a also highlights the scale of the rope clouds compared to the scale of SS93 and demonstrates that cloud band 4 was the leading edge of the cold front from the midlatitudes. An infrared image for the same time (1801 UTC 13 March) shows that the majority of the clouds behind the storm were warm lower-tropospheric clouds, while the bulk of the cloudiness associated with the comma tail was composed of cold, high clouds.

A surface map at 13/18 (Fig. 15) illustrates the extent of the cold air surge. While SS93 was located over the Carolinas, the surface anticyclone was centered just south of BRO. Meanwhile over the eastern Pacific Ocean, the surge penetrated Chivela Pass and into the Gulf of Tehuantepec, supported by a 12-hPa cross-isthmus pressure gradient. Two ships in the Gulf of Tehuantepec (Fig. 15) reported winds of 20 m s^{-1}, consistent with the surface winds from the ECMWF analysis at this location (Figs. 3a and 5a).

By 13/09, there were suggestions of weak prefrontal cloud bands ahead of and parallel to cloud band 5 (e.g., Figs. 12d and 14a). Also the initially symmetric rope cloud (cloud band 5) began to move southwest (Fig. 10). This rotation is consistent with the lower-tropospheric winds from the ECMWF analysis indicating a turning of the jet in time (Figs. 3d, 5a, and 6a). During the period cloud band 5 was unobscured by high clouds associated with convection farther south and the southern extent of the cloud band moved very little from 1700 to 2200 UTC compared to the western edge, which continued to move rapidly westward on 14 March. A similar path for the rope cloud was identified by Parmenter (1970). Continuing with the inertial circle con-

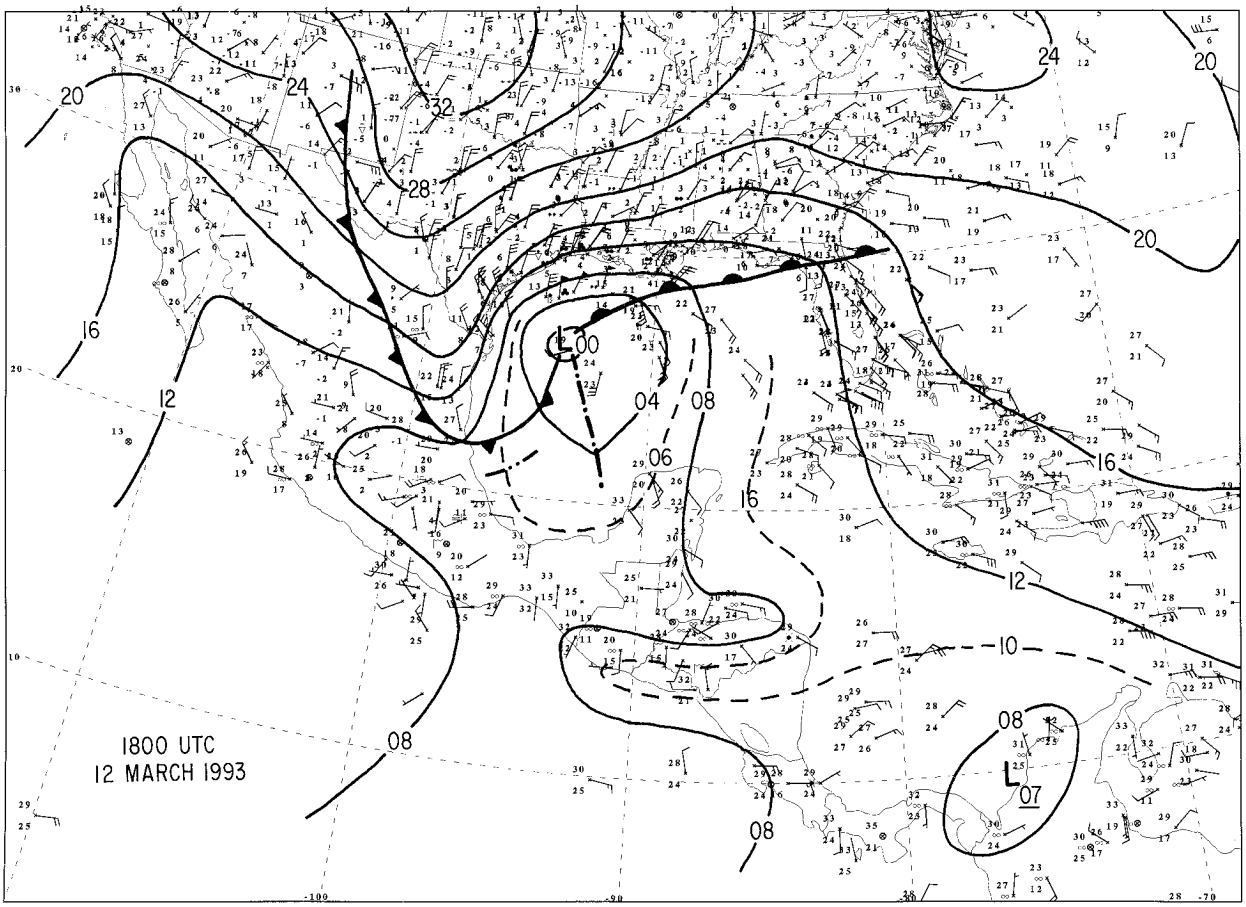

FIG. 13. Manually analyzed surface map for 1800 UTC 12 March. Mean sea level isobars every 4 hPa (solid) and every 2 hPa (dashed, where needed to enhance analysis). Winds: one pennant, full barb, and half-barb denote 25, 5, and 2.5 m s^{-1}, respectively. Conventional frontal analysis and surface station reports. Dash–dot line represents a surface trough and dash–double-dot line represents location of cloud band 2.

cepts from section 4b, the arc of a circle with a radius of 530 km, the radius of an inertial circle at this latitude, originating at the Gulf of Tehuantepec shown in Fig. 10, is very similar to the path of cloud band 5. The poleward portion of cloud band 5 also rotated slower than the equatorward portion, consistent with a smaller inertial radius for a larger value of the Coriolis parameter. The observed rotation rate of cloud band 5 was about 72 h, an inertial period for 9°N, the southernmost extent of cloud band 5. Therefore, the isochrones are qualitatively consistent with an inertial oscillation, but it is possible that other processes (such as advection of the rope cloud by the ambient flow) were also responsible for the movement of the cloud band.

The strong winds from the surge reached Bahias de Huatulco, Mexico (HUX), on the Pacific coast west of the isthmus (Fig. 11f) about 13/18. East winds of 10 m s^{-1} were accompanied by a pressure decrease of about 3 hPa, a dewpoint drop of 9°C, and an elevated temperature (by about 3°C over the maxima on 12 and 14 March). This change appeared to have occurred after cloud band 5 would have already passed HUX much earlier in the day (Figs. 10 and 12d). These observations suggest that the strong wind at HUX was due to air from behind the surge on the east side of the Sierra Madre descending to HUX on the west side.

Another station that experienced the effects of the cold surge was Tuxtla Gutierre, Mexico (TGZ), 528 m above sea level in the highlands on the east side of the Isthmus of Tehuantepec. Frontal passage for TGZ occurred sometime during their normal nighttime cessation of recording observations between 0040 and 1300 UTC 13 March (Fig. 11g). Their weather for the daytime on this day consisted of light drizzle and fog with a maximum temperature of 13°C (15°C colder than the previous day) and 15 m s^{-1} north winds gusting to 20 m s^{-1}.

At 13/18, the winds at San Jose, Guatemala (MGSJ), were primarily southerly keeping MGSJ hazy, hot, and humid (Fig. 11h). At 14/01, the wind shifted to northerly and the dewpoint dropped 12°C in 1 h and the temperature dropped 2°C the following hour, suggestive of downslope flow of the cooler postsurge air. After 12 h of northerlies, the winds returned to southerly; however, the dewpoint did not rebound as quickly as it dropped

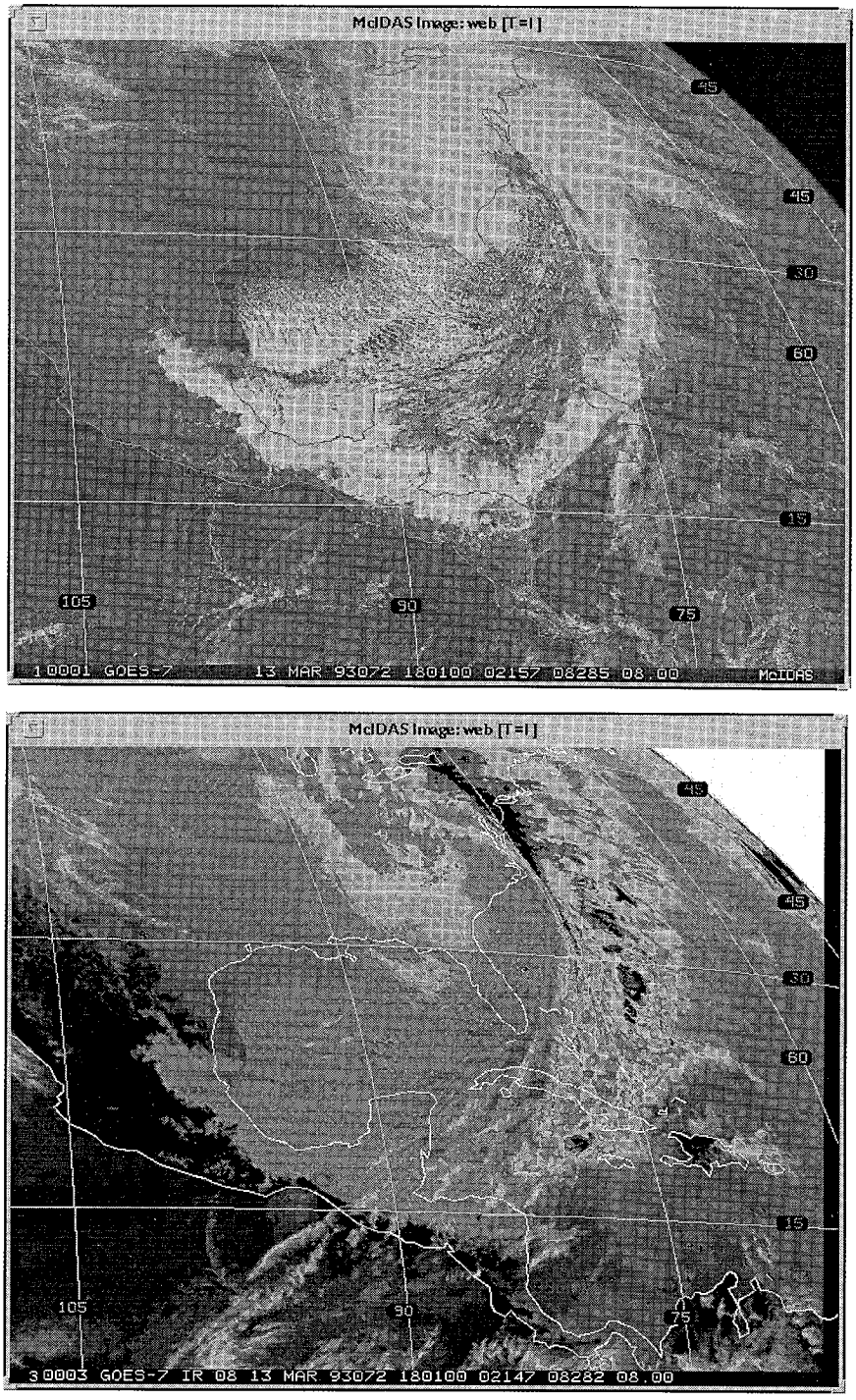

FIG. 14. *GOES-7* satellite imagery of SS93 and the cold surge. 1801 UTC 13 March 1993: (a) visible and (b) infrared, enhanced with operational MB scale (Clark 1983).

since the previously descended dry air over the Pacific Ocean had to return poleward again.

A surface map at 14/18 shows the high pressure confined to the east side of the mountains in Central America (Fig. 16). The pressure gradient across the Isthmus of Tehuantepec was still 6.5 hPa, supporting 10 m s^{-1} winds through the gap. Four-hundred kilometers offshore of Nicaragua, a ship in 15 m s^{-1} winds associated with the papagayo reported blowing sand or dust. The surface temperature at Balboa, Panama (MPHO), had

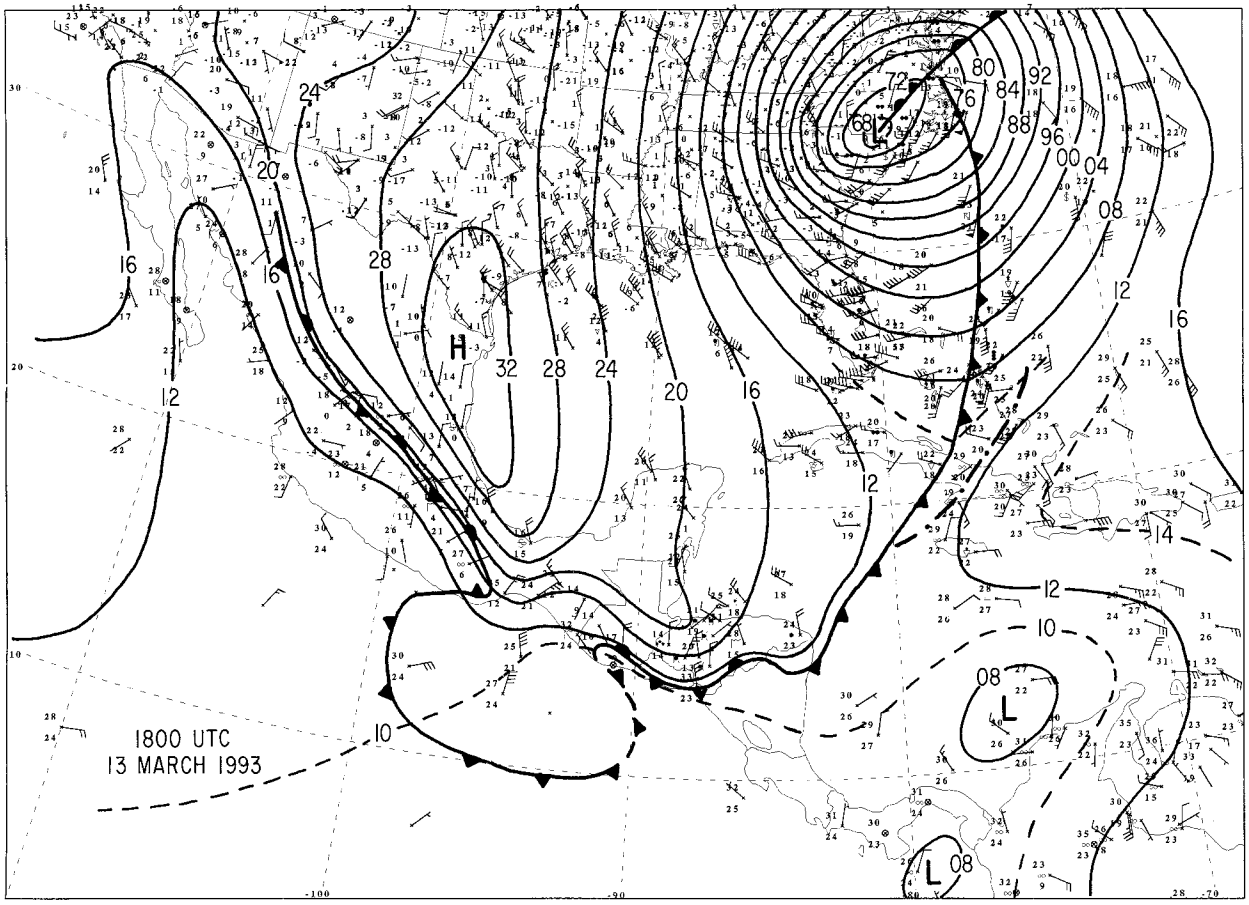

FIG. 15. Manually analyzed surface map for 1800 UTC 13 March. Notation as in Fig. 13 except dash–dot line represents location of a prefrontal squall line. Location of northern squall line discussed by Kocin et al. (1995) is not shown.

dropped 3°C compared to the same time 24 h earlier, indicating a slight cooling in this region. A visible satellite image from the same time shows the low clouds all along the east coast of Central America from Mexico to Panama (Fig. 12e).

The vertical structure of the cold surge can best be illustrated by serial temperature and wind soundings at selected stations (Fig. 17). The approach of the strong winds and cooler temperatures occurred aloft first at VER between 12/12 and 13/00 (Fig. 17a). At 13/00, the lowest 30 hPa was absolutely unstable and the winds were strongest around 900 hPa, consistent with the cross sections from the ECMWF analysis (Fig. 4a). Within the cold air at 13/12 and 14/00 the lowest 70 hPa was well mixed with a nearly constant potential temperature. The depth of the cold air extended up to about 650 hPa and amounted to a cooling of about 14°C, demonstrating the deep synoptic scale of the cold air at this latitude at 13/12. The 25 m s^{-1} winds in the lower troposphere behind the leading edge of the cold surge (Fig. 17a) are consistent with the observed surface wind gusts, indicating that the momentum is likely to have been mixed down in the turbulence behind the cold surge.

The waning of the cold air at VER is documented in Fig. 17b. As shown in Figs. 6–9, an anticyclone moved into the western Gulf of Mexico bringing large-scale subsidence. As seen in Figs. 17a,b, the inversion above the cold lower-tropospheric air descended and became more stable during this period. The development of a lee trough in the central United States at 15/12 (Fig. 9a) caused deep southerlies, warming the lower troposphere above VER (Fig. 17b).

By the time the surge penetrated to Belize City, Belize (MZBZ), the cool air was only about 200 hPa deep with a 11°C decrease, whereas at MPHO, the cooling in the lower troposphere amounted to less than 100 hPa and 1°–2°C (Figs. 17c,d). Despite the arrival of 15 m s^{-1} winds at 800–900 hPa at 15/12, the surface winds at MPHO did not change very much, perhaps due to the predominant northwest channeling of flow through the gap in the mountains through which the Panama Canal lies. By 16/12, there was a 2°C increase in temperature in the lower troposphere above the surface as the wind decreased in speed and veered from the northeast.

To see if the observed pressure change could be due to the arrival of the cold air in the lower troposphere,

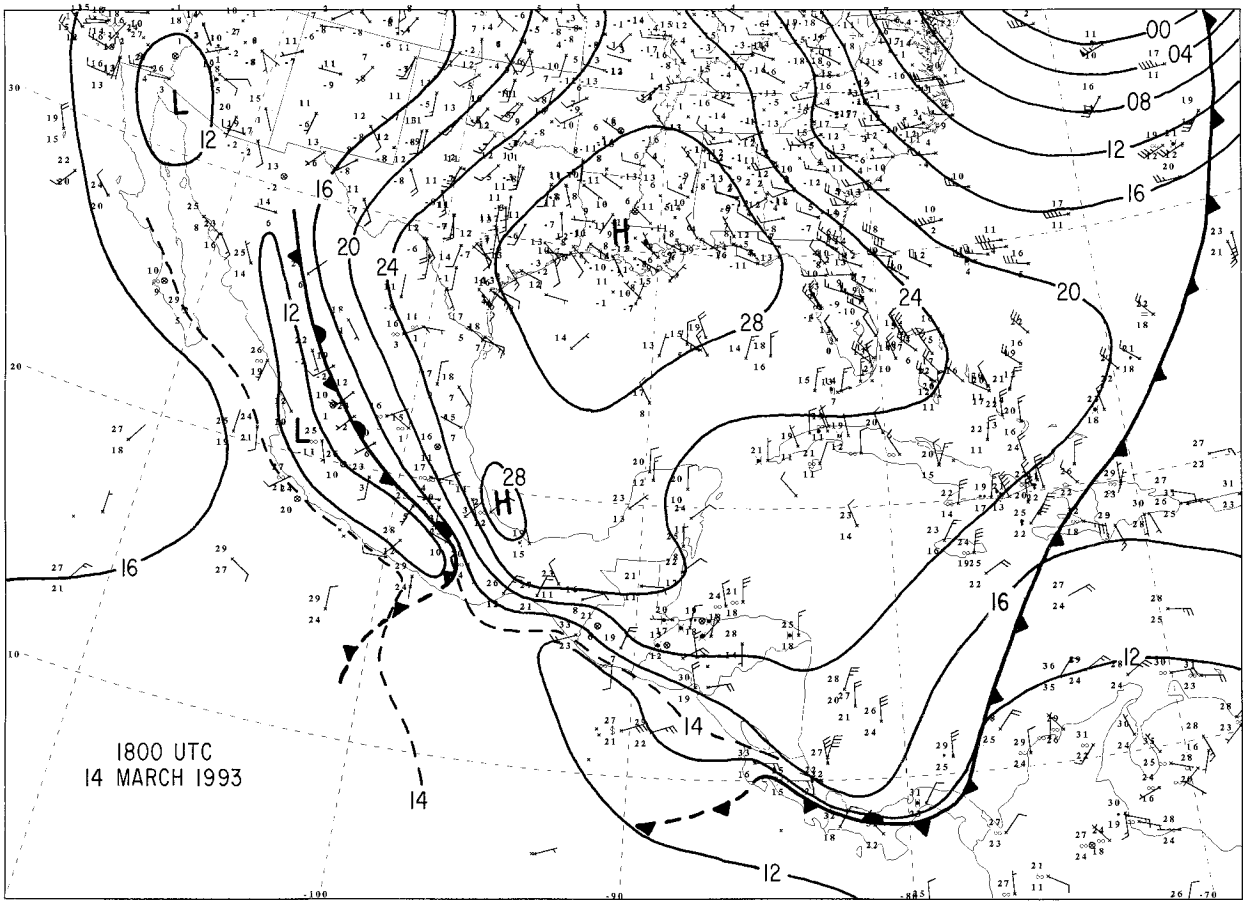

FIG. 16. Manually analyzed surface map for 1800 UTC 14 March. Notation as in Fig. 13.

the depth of the cold air required to produce the observed hydrostatic pressure change attributed to the cold surge at VER and MZBZ was calculated (see appendix). The depth of the cold air that would account for the observed pressure increase was calculated to be 3.8 km for VER (12/12–13/00) and 2.1 km for MZBZ (12/12–13/12). A comparison with Figs. 17a,c shows that the depth of cold air at these times was about 1.5 km for VER and 2 km for MZBZ. Therefore, the increase in surface pressure may be explained by the arrival of the colder denser air in the lower troposphere at MZBZ but not at VER, suggesting that additional adjustment in the air column above VER is likely. This appears to be confirmed by examining the 700-hPa height change at both of these stations, which shows that at VER, the height increased by 21 m, but by only 1 m at MZBZ. The adjustment throughout a deep layer of the atmosphere suggests that the surge (at least at VER) could not simply be a gravity current.

The total precipitation associated with SS93, the cold surge, and tropical convection from 11 to 15 March is displayed in Fig. 18. There was a maximum of precipitation along the east- and north-facing slopes of Mexico and Central America with a local maximum of 79 mm in Honduras associated with the atemporalado. This rain fell during a 2-day period as the area was blanketed in nimbostratus and drizzle (e.g., Fig. 11e). Although only moderate amounts of precipitation (12 mm and less) were reported in Costa Rica, streamflow measurements indicate that several rivers increased their streamflow by 10–20 times their prestorm level (P. Waylen 1996, personal communication). Another precipitation maximum of 119 mm was associated with the squall line over Cuba (Alfonso and Naranjo 1996). The onset of precipitation over Colombia on 14–15 March (a maximum of 99 mm) from convective clouds with very cold temperatures (< -90°C) was coincident with the arrival of the surge into Panama. Unfortunately, the paucity of in situ surface and upper-air observations and the inability of the ECMWF analyses to resolve this convection make it difficult to convincingly document the evolution and environment of this convection.

c. Impact of the cold surge on the eastern Pacific Ocean

The tehuantepecer and papagayo wind events also had an impact on the SSTs in the eastern Pacific Ocean.

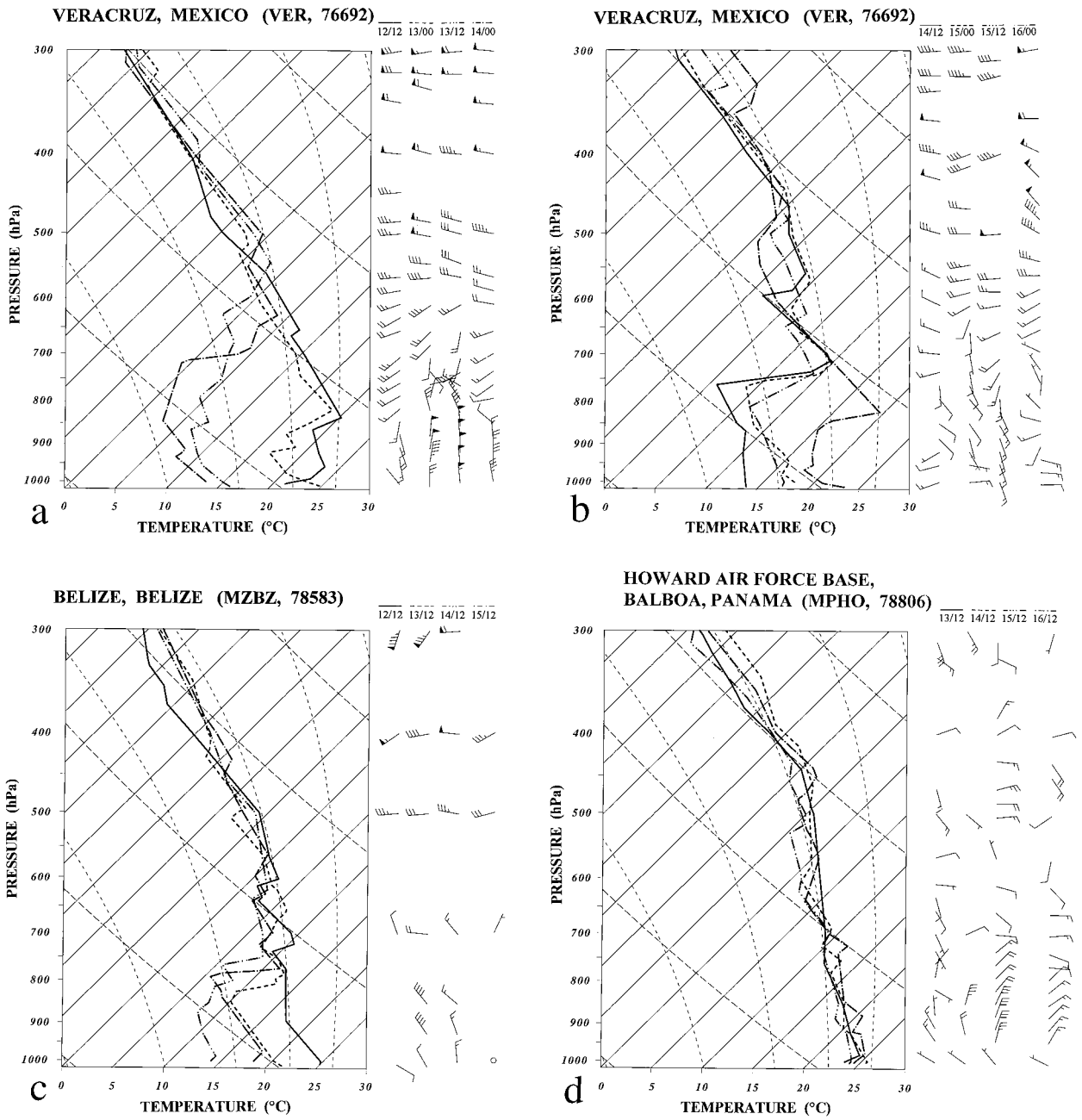

FIG. 17. Serial temperature and wind profiles before, during, and after surge passage. (a) Veracruz, Mexico (VER, 76692): 1200 UTC 12 March, 0000 UTC 13 March, 1200 UTC 13 March, and 0000 UTC 14 March. (b) Veracruz: 1200 UTC 14 March, 0000 UTC 15 March, 1200 UTC 15 March, and 0000 UTC 16 March. (c) Belize City, Belize (MZBZ, 78583): 1200 UTC 12 March, 1200 UTC 13 March, 1200 UTC 14 March, and 1200 UTC 15 March. (d) Howard Air Force Base, Balboa, Panama (MPHO, 78806): 1200 UTC 13 March, 1200 UTC 14 March, 1200 UTC 15 March, and 1200 UTC 16 March.

Figure 19 illustrates the SST before and during the gap wind events. These values of SST represent infrared brightness (skin) temperatures over cloud-free areas and for SS93 were generally 5°C colder than in situ SST measurements (not shown). Hence, the values in Fig. 19 should only be used in a relative and not an absolute sense. At 2101 UTC 12 March, temperatures in the Gulf of Tehuantepec, generally 23°–24°C (Fig. 19a), are already 1°–2°C cooler than other coastal areas, probably from the cold surge during the previous week. Nearly 2 days later, at 1801 UTC 14 March, a 6°–8°C cooling occurred just offshore of Mar Muerto and a mushroom-

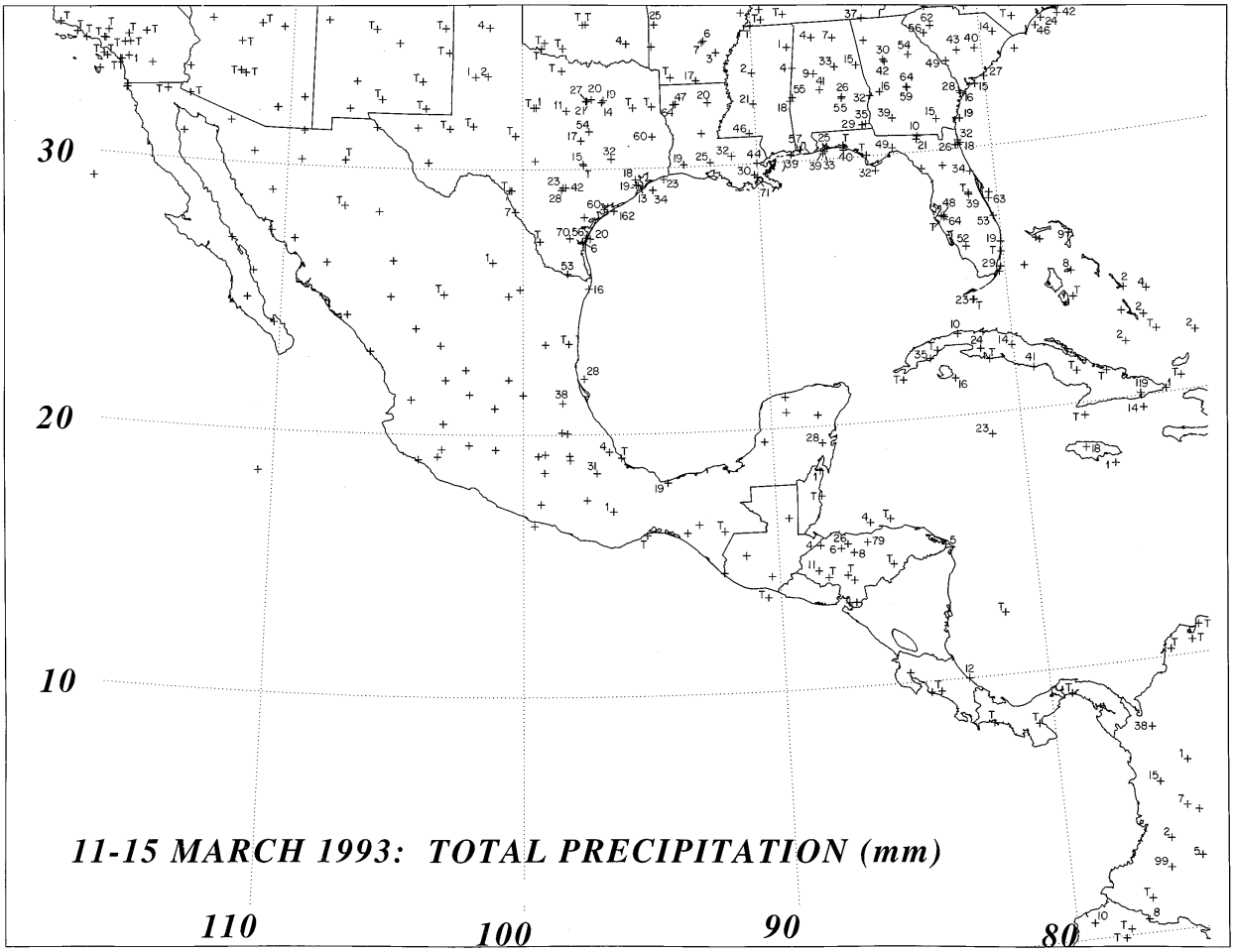

FIG. 18. Total precipitation (mm) from SS93, cold surge, and tropical convection, 11–15 March 1993, determined by the addition of daily precipitation values. Available stations are marked with a cross; T = trace. Precipitation is measured from 0600 UTC 11 March to 0600 UTC 16 March for stations in the United States, 0000 UTC 11 March to 0000 UTC 16 March for stations in Mexico and Central America, and 1200 UTC 11 March to 1200 UTC 16 March for stations in South America.

shaped patch of cool water appeared (Fig. 19b). Clarke (1988, p. 15 500) has also noted this mushroom shape and has suggested that it may result from the projection of the oceanic jet (or squirt) formed by the tehuantepecer into relatively quiescent water. Cooling of the SSTs by about 4°–6°C occurred off the Nicaragua coast associated with the papagayo. In situ ship observations of SST before the tehuantepecer were generally about 28°–30°C (not shown). Even after the event, most temperatures were still greater than 27°C, but on 16 March, a temperature of 22°C was observed in the region of oceanic cooling in Fig. 19b by a ship at 14°N, 95°W. At this early stage in the evolution of the oceanic response to the tehuantepecer (Fig. 19b), the cool squirt was shaped relatively symmetric with a slight southwest–northeast (or anticyclonic) trend, resembling squirts observed in other studies. Observations of squirts formed by tehuantepecers indicate a preference for more intense SST gradients on the west side of the oceanic jet (e.g., Clarke 1988) and are consistent with those from 1801 UTC 14 March (Fig. 19b). Clarke (1988) attributed this asymmetry to Ekman convergence on the right side of the squirt. Therefore, the squirt and cooler upwelled water are consistent with previous observations of the oceanic response to tehuantepecers.

d. Summary

Employing observational data in the mesoscale analysis of the cold surge associated with SS93 led to the following conclusions. While the surge was moving along the east side of the Sierra Madre in central and southern Mexico, the frontal structure of the leading edge of the cold surge did not resemble the classic structure of a cold front (e.g., Sanders 1955). In particular, two aspects differed from the classic model: the tipped-forward nature of the leading edge and the presurge cloud bands. Vertical profiles through the surge in eastern Mexico indicate that the cold advection and strong winds at 925 hPa preceded the arrival of the cold north-

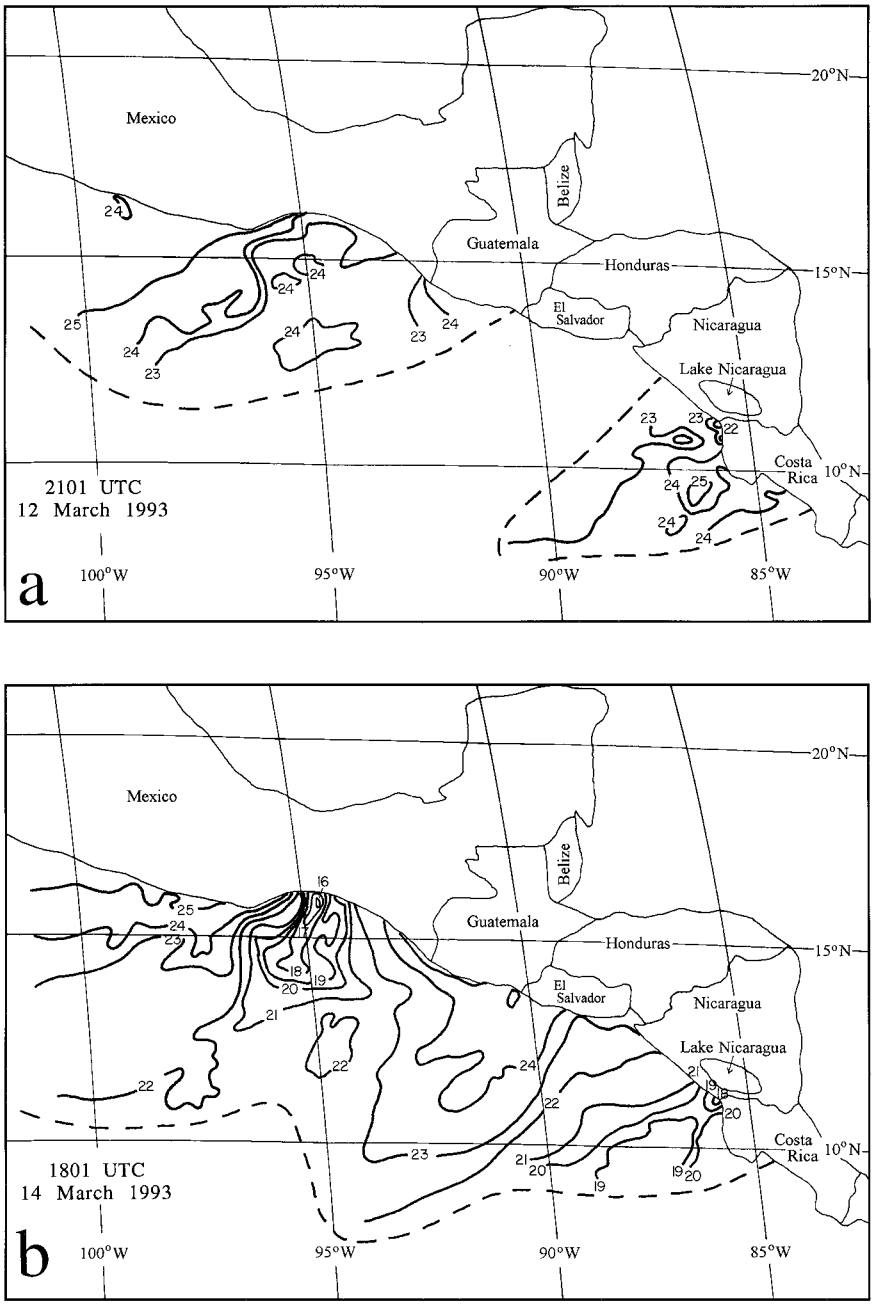

FIG. 19. Sea surface temperatures (°C) derived from 4-km-resolution infrared-imagery brightness temperatures. Dashed lines enclose areas of reliable cloud-free infrared values. Values are generally 5°C colder than in situ measurements and so should only be used in a relative sense, not an absolute sense: (a) 2101 UTC 12 March and (b) 1801 UTC 14 March.

erlies at the surface. The multiple rope clouds, likely representing localized surface convergence, formed as the surge progressed equatorward. They were characterized by spatial scales of 10–30 km in the cross-front direction and 100–800 km in the along-front direction and moved at a speed approximately equal to the wind speed behind the surge (~15–20 m s^{-1}). New rope clouds (presurge cloud bands) appeared to form as a developing boundary in the warm air 150–200 km ahead of the surge. Eventually the new rope clouds became associated with the leading edge of colder, higher, momentum air, supplanting the old surge line. Recognizing the limitations of our data, we estimate that some of the rope clouds appeared to have a lifetime of 6–10 h before dissipating.

As the surge progressed farther equatorward, an ac-

celeration of the cold surge occurred in eastern Honduras/northern Nicaragua, creating a bend in the associated rope cloud (cloud band 4). This acceleration appears to be related to the change in orientation of the topography in this region. The other rope cloud at this time, cloud band 5 associated with the tehuantepecer, rotated anticyclonically, consistent with previous observations (Parmenter 1970) and is likely attributed to an inertial oscillation (Clarke 1988).

Finally, the surge impacted the Tropics by producing an atemporalado, yielding as much as 79 mm of postfrontal rain over topographically favorable regions (e.g., mountainous regions of Honduras). Also, sea surface temperature decreases up to 6°–8°C occurred within the span of several days and confirm in situ observations of SST decreases associated with previous CACS events (see section 2c).

6. Discussion

Observations from this CACS are consistent with other observations from historical cold surges (e.g., Hurd 1929; McBryde 1932), suggesting that this event was typical of strong cold surges in Central America and Mexico. In this section, concepts discussed briefly within this paper are elaborated upon and the observations are related to those of previous investigators.

a. The structure of cold fronts in the Tropics

In section 1b, previous conceptualizations of cold fronts in the Tropics associated with the leading edges of CACSs were briefly described. For the surge associated with SS93, many of these ideas appear to be consistent with the observations.

For instance, one hypothesis proposed that cold fronts lose their identity and are better described as shear lines deep in the Tropics (e.g., Mosiño Alemán and García 1974, p. 357; Reding 1992, 10–13). Figure 17 supports this interpretation. Compared to passage at MZBZ and VER, the degree of cooling in the lower troposphere at MPHO was significantly less with the CACS passage, yet the strong winds remain a deep feature. But as the surge associated with SS93 attests, the leading edge of cold surges can remain intact after crossing into Mexico, despite generating presurge cloud bands and thereby demonstrates that midlatitude cold fronts can attain longevity approaching several days despite advancing deep into the Tropics.

Another hypothesis is that the front separates into two portions: the density discontinuity, or shear line, and the pressure trough (e.g., Palmer 1951, p. 867; Trewartha 1966, p. 46; Fermor 1971). This is consistent with the observations discussed in section 5, which describe the evolution of the presurge cloud bands. In this case, the lowest pressure was usually not colocated with the onset of the strongest pressure rises, the most rapid temperature drop, and the strongest northerlies, but instead preceded them by several hours and 150–200 km. It was apparent that the leading edge of the surge in coastal eastern Mexico reformed in the prefrontal air. Further discussion of the similarity of this feature to conceptual models of mesoscale frontal structure can be found in section 6b.

A third hypothesis suggested that midlatitude cold fronts arrive as fronts aloft first and may later become evident at the surface (e.g., Forsdyke 1949; Palmer 1951, p. 867; Trewartha 1966, 46–48); the soundings in Fig. 17 suggest this possibility. As has been previously noted in sections 4 and 5, the strongest winds and cooling at VER arrive at approximately 900 hPa first, consistent with other cases of midlatitude cold fronts (e.g., Kuo and Reed 1988; Mass and Schultz 1993; Colle and Mass 1995, their Fig. 17). Possible explanations for this tipped-forward frontal structure may include one or more of the following: surface friction, adiabatic cooling in the leading edge updraft, turbulent mixing in the lowest layer of the atmosphere, and differential frontal movement across a prefrontal inversion.

1) The impact of surface friction on cold fronts appears to occur on a scale much smaller than that observed here. Shapiro (1984) showed that the forward tilt of the front owing to frictional retardation amounted only to about 50 m in the lowest 50–100 m above the surface in this case. While friction is likely affecting the structure of the surge in this case, the available data are not of sufficient resolution to ascertain its effect. In addition, even if it were possible to observe this structure, the depth of the observed tilt was greater by an order of magnitude than that observed by Shapiro.
2) Cooling aloft by adiabatic ascent is a possibility in this case since the ascent is coincident with the leading edge of the cooler air (e.g., Figs. 8a,c). The moist-adiabatic ascent of prefrontal surface air at VER to 900 hPa, however, results only in a temperature of about 20°C, compared to the 17°–18°C air at that level at 13/00 (Fig. 17a). Therefore, it is likely that adiabatic lifting cannot explain all of the cooling.
3) Turbulent mixing in the presence of a warm lower boundary may explain both the superadiabatic lapse rate near the surface of the earth and, thus, the forward tilt of the thermal boundary, but not the forward tilt of the wind speed maximum (Figs. 4a and 17a,c,d).
4) The presence of the subsidence inversion associated with the subtropical high around 850 hPa may act to usher in the cold, high momentum air more readily above, rather than below, the inversion as described by Bedard and Sanders (1978). This process was believed to be important in cases described by Hardy et al. (1973) (R. Reed 1989, personal communication) and Bedard and Sanders (1978). As seen in Fig. 17a, the 25 m s^{-1} northerlies at VER arrive first at

the level of the inversion at 13/00, suggesting the validity of this idea. A weakness in this hypothesis is that the mechanism by which mixing is inhibited by the inversion at the leading nose of the surge aloft, but occurs farther back in the cold air despite the presence of the inversion, has not been conclusively demonstrated.

Thus, several hypotheses have been proposed for the tipped-forward structure of the surge, but none alone appear adequate to explain the frontal structure as ascertained from the observational data and the ECMWF analysis.

Two ideas that do not appear to hold for the CACS associated with SS93 follow. Portig (1959) believed that the transition between air masses occurs gradually and therefore the term ''front'' is not appropriate for midlatitude fronts that reach the Tropics, and Palmer (1951, p. 867) claimed that these fronts are destroyed shortly after entering the Tropics. The leading edge of the surge associated with SS93, however, was quite sharp at times, bearing strong winds and cool temperatures. Clearly, these ideas do not apply to the CACS associated with SS93.

b. Presurge cloud bands

On the mesoscale, the leading edge of the surge associated with SS93 was not a classic cold front (e.g., Sanders 1955) owing to the presurge pressure troughs and cloud bands at various times during its evolution, as well as its tipped-forward structure. Tepper (1950), Newton (1950), Trewartha (1966, p. 46), Hanstrum et al. (1990a,b), Hutchinson et al. (1994), and Sanders and Doswell (1995), among others, have recognized the importance of such prefrontal features. Possible explanations for prefrontal cloud bands include Kelvin waves, turbulent mixing at the leading edge, pressure-jump lines, bores, and gravity currents.

One hypothesis is that the presurge cloud bands may be solitary Kelvin waves. Among the evidence in support of Kelvin waves is that the presurge cloud bands move equatorward on the east side of the Sierra Madre and are isolated features that propagate faster than the advective wind speed (15 m s^{-1} vs 10 m s^{-1}). But Kelvin wave theory is inadequate to explain why the presurge cloud band should become the leading edge of the surge after 6–10 h.

Alternatively, turbulent mixing associated with the tipped-forward structure of the surge may be producing the presurge cloud bands; in other words, cooler, higher-momentum air from the nose of cold air aloft becomes mixed downward. This would explain why the prefrontal surge became the dominant surge over time, but since information about how far the cold nose was ahead of the leading edge of the surge at the surface is lacking from the observations (the ECMWF analyses suggest up to 200 km at different stages in the evolution of the cold surge), further speculation cannot be made.

Another hypothesis to explain the presurge cloud bands is a pressure-jump line. Tepper (1950) proposed that accelerating cold fronts produced pressure jumps that propagated along an elevated inversion in the prefrontal air and were associated with squall lines. He did not address, however, the mechanism of what induces the acceleration of the cold front. The pressure jump lines are not characterized by a uniform pressure increase, but a rapid pressure rise and fall, returning to *steady* higher pressures after the jump than before. VER was the only station in which this stabilization of the pressure behind the prefrontal trough was observed, although the available data may not be sufficient to determine this conclusively. Consequently, we cannot conclude whether or not pressure jump lines are similar to the mesoscale prefrontal troughs associated with SS93.

Somewhat related to pressure-jump lines are bores generated by gravity (density) currents in laboratory experiments and numerical model simulations (e.g., Simpson 1987). In particular, for gravity currents moving into prefrontal surface-based stable layers, disturbances can form on the stable layer (bores), and if these bores have large enough amplitude, they may resemble gravity currents (e.g., Rottman and Simpson 1989; Haase and Smith 1989). Were this to occur, it is likely that the bore would remain separated from the main source of colder air and, hence, could not be similar to the presurge cloud bands observed in this case since the presurge cloud bands later became the main surge. We are unaware of modeling experiments with elevated prefrontal stable layers that more closely resemble the conditions in this case. Similar presurge cloud heads appear to have been observed in two-dimensional simulations of gravity currents in uniform shear flows (e.g., Chen 1995), but the applicability to this case is unclear.

Another requirement of a gravity current is that the lower layers must have front-to-rear relative flow; in other words, the wind speed behind the front must exceed the speed of the front itself (e.g., Smith and Reeder 1988). In the surge associated with SS93, the average speed of cloud band 1 over a 7-h period was about 20 m s^{-1} (with a variability of 15–30 m s^{-1} as measured from hourly position changes in Fig. 10), which was nearly the strength of the winds in the lower troposphere behind the surge. For cloud band 2, the average speed was measured to be about 15 m s^{-1} (or 6–22 m s^{-1} for hourly rates), whereas the surface winds behind the cloud band were about 10 m s^{-1}. Because the question of what the appropriate frontal speed and postfrontal wind velocity to use might be, this test is inconclusive. Therefore the gravity current model can explain some, but not all, of the observations in the surge associated with SS93.

Consequently none of these proposed conceptual models adequately explain all the available observations for the presurge cloud bands identified during the cold

surge associated with SS93. Mesoscale numerical model simulations of this case, currently being performed, may be able to elaborate on the structure, evolution, and dynamics of the presurge cloud bands.

c. Relationship to Colle and Mass (1995)

In this section, the relationship between the CACS associated with SS93 is compared to the cold surges discussed by Colle and Mass (1995). The initiation of the cold surge is consistent with the results of Colle and Mass (1995), who attributed the onset of a cold surge to a process similar to cold-air damming. Ultimately this change in orientation of the isobars, which triggered the onset of the cold surge, was related to the evolution of the synoptic pattern. Specifically, for the surge associated with SS93, the change was crucially dependent on the arrival of PV anomaly C associated with the jet streak aloft, which then permitted the cyclone in the lee of the Sierra Madre to deepen and move eastward. With the cyclone to the east, the anticyclone was then free to move equatorward. In the case presented by Colle and Mass (1995), however, the lee trough weakened in situ, never developing into a cyclone before being overtaken by the surge.

The equatorward progress of the surge associated with SS93 was likely aided by low-latitude synoptic forcing associated with PV anomaly C, as well as the ageostrophic secondary circulation associated with the jet entrance region in the upper troposphere. Hence, there appears to be some large-scale dynamical, as well as topographic, control over cold surges. This point is underscored by Colle and Mass (1995), who selected cases in which the upper-tropospheric flow was weak and zonal from Texas southward (B. Colle 1995, personal communication). In fact, the surge studied by Colle and Mass (1995) never even reached MID (Reding 1992) or the Isthmus of Tehuantepec (B. Colle 1995, personal communication). The lack of low-latitude forcing allowed them to attempt to isolate the topographical processes from large-scale dynamics. In the surge associated with SS93, synoptic forcing associated with PV anomaly C was present to much lower latitudes (Fig. 3d) than the cases discussed in Colle and Mass (1995). These issues are explored in a future paper showing that the strength and longevity of CACSs depend on the planetary- and synoptic-scale flow over North America and the eastern Pacific Ocean.

7. Summary

Therefore to summarize the cold surge associated with SS93, we believe that the surge was extraordinary partly owing to topographic channeling and partly owing to the dynamics associated with the low-latitude short-wave trough and confluent jet entrance region, favoring the deep penetration of the surge into the Tropics. The cold surge appeared to arrive in the Tropics first as an abrupt mesoscale boundary, but also later as a synoptic-scale cold surge where cooler, higher-pressure air continued to invade the Tropics.

On the mesoscale, the structure and evolution of the cold surge were not similar to those of classic cold fronts throughout its duration because of its tipped-forward leading edge and the appearance of multiple presurge cloud bands. The origin and dynamics of the presurge cloud bands bear some resemblance to structures previously discussed in the literature such as Kelvin waves, turbulent mixing at the leading edge, pressure-jump lines, bores, and gravity currents, but the presurge cloud bands observed with the cold surge associated with SS93 do not appear to satisfactorily fit these conceptual models.

The movement of the surface cyclone and anticyclone was also responsible for the timing of the onset and the cessation of the strong gap winds observed in the Gulfs of Tehuantepec, Fonseca, Papagayo, and Panama. The anticyclonic turning of the rope cloud in the Gulf of Tehuantepec appeared to be a response to the Coriolis torque on a near-surface jet, resulting in an inertial oscillation.

Finally, the impact of the cold surge on the Tropics was to generate heavy, orographically enhanced precipitation, enhancement of the northeast trade winds over the eastern Pacific Ocean, and cooling of the sea surface temperature offshore of Mexico and Central America.

Acknowledgments. This paper grew out of a graduate synoptic-dynamic laboratory class devoted to a multiscale analysis of the superstorm of March 1993. We are deeply indebted to the following individuals for their contributions to this work: Barry Schwartz of the Forecast Systems Laboratory for providing observations from Central America and Mexico; Drs. Gary Lackmann of McGill University and Haig Iskenderian of Atmospheric and Environmental Research, Inc., for assistance in obtaining ECMWF analyses and other data; Matthew Pyle of SUNYA for assistance in employing the methodology of Loughe et al. (1995) for this case; Prof. John Horel of the University of Utah for making the NMC model grids for SS93 available on the internet in real time; Anton Seimon of SUNYA for allowing access to his surface mesoanalyses of SS93; Prof. Jim Steenburgh of the University of Utah and Prof. Michael Reeder of Monash University for their advice and comments; Guillermo Quiros Alvarez from the Oceanography and Coastal Management Laboratory of the Universidad Nacional de Costa Rica for providing references on the impact of tehuantepecers on the ocean and imagery of other oceanic cooling events; Prof. James McGuirk of Texas A&M University for generously providing a copy of Reding (1992); Dr. David Fitzjarrald of SUNYA for providing relevant references on northers and data made available by the Universidad Veracruzana and Mexican Weather Service; Drs. Armando Trasviña of the Centro de Investigación Científica y de Educación Superior de

Ensenda, Sam Houston and David Enfield of the National Oceanic and Atmospheric Administration Atlantic Oceanographic and Meteorological Laboratories and, Prof. Peter Waylen of the University of Florida for their advice and interest in this project; Jennifer Miletta of the Pacific Marine Environmental Laboratory (PMEL) for advice on the interpretation of satellite imagery; Dr. Robert Atlas and Joseph V. Ardizzone of the NASA Goddard Space Flight Center for providing SSM/I and *ERS-1* wind data; Marilyn Peacock for drafting some of the figures; and Brian Colle of the University of Washington, Dr. Fred Sanders, and the anonymous reviewers whose comments helped improve this manuscript.

We are grateful to ECMWF, SSEC, PMEL, and the Data Support Section of the Scientific Computing Division of NCAR for providing data used in this study. All gridded and observational data were stored, analyzed, and displayed using the Generalized Meteorological Analysis Package (GEMPAK; Koch et al. 1983), a product of the National Aeronautics and Space Administration and National Centers for Environmental Prediction (NCEP, formerly NMC). Digital satellite imagery was displayed and manipulated with the Man–Computer Interactive Data Access System (McIDAS; Suomi et al. 1983).

This research was supported by the National Science Foundation through Grant ATM-9413012 and the National Oceanic and Atmospheric Administration through Grant NA56GP0197 awarded to the State University of New York at Albany.

APPENDIX

Calculation of Hydrostatic Pressure Changes

To calculate the depth of cold air responsible for the observed hydrostatic pressure changes at VER and MZBZ, Schoenberger's (1984) formula was employed:

$$\Delta P = \frac{Pg\Delta Z\Delta T_v}{RT_{vw}T_{vc}}, \qquad \text{(A1)}$$

where ΔP is an estimate of the hydrostatic surface pressure rise behind the front, P is the environmental (presurge) pressure, g is gravity, ΔZ is the depth of the cold air, T_{vw} is the mean virtual temperature of the warm air, T_{vc} is the mean virtual temperature of the cold air, $\Delta T_v = T_{vw} - T_{vc}$, and R is the gas constant for dry air. Solving for ΔZ, the equivalent depth of cold air to account for the observed pressure rise can be calculated at different observing stations.

For VER between 12/12 and 13/00, $\Delta P = 6$ hPa, $P = 1005$ hPa, $T_{vc} = 292 \pm 1$ K, and $T_{vw} = 296 \pm 3$ K. Examination of T_v profiles (similar to Fig. 17a) suggests that realistic values of ΔT_v are about 3–5 K, consistent with an average ΔT_v calculated from the 850–1000-hPa thickness change (4.0 K). Using these values produced $\Delta Z = 3.8 \pm 1.2$ km.

For MZBZ between 12/12 and 13/12, $\Delta P = 5$ hPa, $P = 1008$ hPa, $T_{vc} = 290 \pm 6$ K, and $T_{vw} = 296 \pm 5$ K. Examination of T_v profiles (similar to Fig. 17c) suggests that realistic values of ΔT_v in the lowest 150 hPa are about 5–6 K. The 850-hPa height at 12/12 was missing, making an independent check from the thickness impossible. Using these values produced $\Delta Z = 2.1 \pm 0.4$ km.

REFERENCES

Alfonso, A. P., and L. R. Naranjo, 1996: The 13 March 1993 severe squall line over western Cuba. *Wea. Forecasting*, **11,** 89–102.

Baines, P. G., 1980: The dynamics of the southerly buster. *Aust. Meteor. Mag.*, **28,** 175–200.

Barton, E. D., M. L. Argote, J. Brown, P. M. Kosro, M. Lavin, J. M. Robles, R. L. Smith, A. Trasviña, and H. S. Velez, 1993: Supersquirt: Dynamics of the Gulf of Tehuantepec, Mexico. *Oceanography,* **6,** 23–30.

Bedard, A. J., Jr., and M. J. Sanders, Jr., 1978: Thunderstorm-related wind shear detected at Dulles International Airport using a Doppler acoustic/microwave radar, a monostatic sounder and arrays of surface sensors. *Proc. Conf. on Weather Forecasting and Analysis and Aviation Meteorology,* Silver Spring, MD, Amer. Meteor. Soc., 347–352.

Beebe, R. G., and F. C. Bates, 1955: A mechanism for assisting in the release of convective instability. *Mon. Wea. Rev.,* **83,** 1–10.

Bell, G. D., and L. F. Bosart, 1988: Appalachian cold-air damming. *Mon. Wea. Rev.*, **116,** 137–161.

Bluestein, H. B., 1977: Synoptic-scale deformation and tropical cloud bands. *J. Atmos. Sci.*, **34,** 891–900.

Bosart, L. F., and B. E. Schwartz, 1979: Autumnal rainfall climatology of the Bahamas. *Mon. Wea. Rev.*, **107,** 1663–1672.

——, G. J. Hakim, K. R. Tyle, M. A. Bedrick, W. E. Bracken, M. J. Dickinson, and D. M. Schultz, 1996: Large-scale antecedent conditions associated with the 12–14 March 1993 cyclone (''Superstorm '93'') over Eastern North America. *Mon. Wea. Rev.*, **124,** 1865–1891.

Boyle, J. S., and T.-J. Chen, 1987: Synoptic aspects of the wintertime East Asian monsoon. *Monsoon Meteorology,* C.-P. Chang and T. N. Krishnamurti, Eds., Oxford University Press, 125–160.

Caplan, P. M., 1995: The 12–14 March 1993 superstorm: Performance of the NMC global medium-range model. *Bull. Amer. Meteor. Soc.,* **76,** 201–212.

Chang, C.-P., J. E. Erickson, and K. M. Lau, 1979: Northeasterly cold surges and near-equatorial disturbances over the winter MONEX area during December 1974. Part I: Synoptic aspects. *Mon. Wea. Rev.*, **107,** 812–829.

——, J. E. Millard, and G. T. J. Chen, 1983: Gravitational character of cold surges during winter MONEX. *Mon. Wea. Rev.,* **111,** 293–307.

Chapel, L. T., 1927: Winds and storms on the Isthmus of Panama. *Mon. Wea. Rev.*, **55,** 519–530.

Chen, C., 1995: Numerical simulations of gravity currents in uniform shear flows. *Mon. Wea. Rev.*, **123,** 3240–3253.

Clark, J. D., 1983: *The GOES User's Guide*. U.S. Department of Commerce, 164 pp.

Clarke, A. J., 1988: Inertial wind path and sea surface temperature patterns near the Gulf of Tehuantepec and Gulf of Papagayo. *J. Geophys. Res.*, **93,** 15 491–15 501.

Clemente-Colón, P., and P. Chang, 1995: Central American CoastWatch? *Mar. Wea. Log,* **39,** 34–35.

Colle, B. A., and C. F. Mass, 1995: The structure and evolution of cold surges east of the Rocky Mountains. *Mon. Wea. Rev.*, **123,** 2577–2610.

Dallavalle, J. P., and L. F. Bosart, 1975: A synoptic investigation of anticyclogenesis accompanying North American polar air outbreaks. *Mon. Wea. Rev.,* **103,** 941–957.

Davis, C. A., 1995: Observations and modeling of a mesoscale cold surge during WISPIT. *Mon. Wea. Rev.,* **123,** 1762–1780.

DeAngelis, R. M., and Coauthors, 1993: Was it the storm of the century? *Mar. Wea. Log,* **37**(2), 38–45.

Dickinson, M. J., M. A. Bedrick, W. E. Bracken, L. F. Bosart, G. J. Hakim, D. M. Schultz, and K. R. Tyle, 1995: Superstorm '93: Synoptic scale precursors and NMC model performance. Preprints, *14th Conf. on Weather Analysis and Forecasting,* Dallas, TX, Amer. Meteor. Soc., 13–16.

DiMego, G. J., L. F. Bosart, and G. W. Endersen, 1976: An examination of the frequency and mean conditions surrounding frontal incursions into the Gulf of Mexico and Caribbean Sea. *Mon. Wea. Rev.,* **104,** 709–718.

Ding, Y., 1994: *Monsoons over China.* Kluwer Academic, 432 pp.

Dorman, C. E., R. C. Beardsley, and R. Limeburner, 1995: Winds in the Strait of Gibraltar. *Quart. J. Roy. Meteor. Soc.,* **121,** 1903–1921.

Fermor, J. H., 1971: The weather during northers at Kingston, Jamaica. *J. Trop. Geogr.,* **32,** 31–37.

Fitzjarrald, D. R., 1986: Slope winds in Veracruz. *J. Climate Appl. Meteor.,* **25,** 133–144.

Flierl, G. R., M. E. Stern, and J. A. Whitehead Jr., 1983: The physical significance of modons: Laboratory experiments and general integral constraints. *Dyn. Atmos. Oceans,* **7,** 233–263.

Forbes, G. S., R. M. Blackall, and P. L. Taylor, 1993: ''Blizzard of the century''—The storm of 12–14 March 1993 over the eastern United States. *Meteor. Mag.,* **122,** 153–162.

Forsdyke, A. G., 1949: Weather forecasting in tropical regions. *Geophys. Mem.,* **82,** 82.

Fortune, M. A., and V. E. Kousky, 1983: Two severe freezes in Brazil: Precursors and synoptic evolution. *Mon. Wea. Rev.,* **111,** 181–196.

Frankenfield, H. C., 1917: ''Northers'' of the Canal Zone. *Mon. Wea. Rev.,* **45,** 546–550.

Garcia, I. P., 1996: Major cold air outbreaks affecting coffee and citrus plantations in the eastern and northeastern Mexico. *Atmósfera,* **9,** 47–68.

Garcia, O., L. Bosart, and G. DiMego, 1978: On the nature of the winter season rainfall in the Dominican Republic. *Mon. Wea. Rev.,* **106,** 961–982.

Gilhousen, D. B., 1994: The value of NDBC observations during March 1993's ''Storm of the Century.'' *Wea. Forecasting,* **9,** 255–264.

Goldbrunner, A. W., 1963: *Las Causas Meteorológicas de las Lluvias de Extraordinaria Magnitud en Venezuela* (Meteorological Causes of Rains of Extraordinary Magnitude in Venezuela). 2d ed. Ministerio de la Defensa, Venezuela, 230 pp.

Haase, S. P., and R. K. Smith, 1989: The numerical simulation of atmospheric gravity currents. Part II. Environments with stable layers. *Geophys. Astrophys. Fluid Dyn.,* **46,** 35–51.

Hakim, G. J., L. F. Bosart, and D. Keyser, 1995: The Ohio Valley wave-merger cyclogenesis event of 25–26 January 1978. Part I: Multiscale case study. *Mon. Wea. Rev.,* **123,** 2663–2692.

——, D. Keyser, and L. F. Bosart, 1996: The Ohio Valley wave-merger cyclogenesis event of 25–26 January 1978. Part II: Diagnosis using quasigeostrophic potential vorticity inversion. *Mon. Wea. Rev.,* **124,** 2176–2205.

Hanstrum, B. N., K. J. Wilson, and S. L. Barrell, 1990a: Prefrontal troughs over Southern Australia. Part I: A climatology. *Wea. Forecasting,* **5,** 22–31.

——,——, and——, 1990b: Prefrontal troughs over Southern Australia. Part II: A case study of frontogenesis. *Wea. Forecasting,* **5,** 32–46.

Hardy, K. R., R. J. Reed, and G. K. Mather, 1973: Observation of Kelvin–Helmholtz billows and their mesoscale environment by radar, instrumented aircraft, and a dense radiosonde network. *Quart. J. Roy. Meteor. Soc.,* **99,** 279–293.

Hartjenstein, G., and R. Bleck, 1991: Factors affecting cold-air outbreaks east of the Rocky Mountains. *Mon. Wea. Rev.,* **119,** 2280–2292.

Hastenrath, S. L., 1967: Rainfall distribution and regime in Central America. *Arch. Meteor. Geophys. Bioklimatol. Ser. B,* **15,** 201–241.

Hayes, S. P., L. J. Mangum, J. Picaut, A. Sumi, and K. Takeuchi, 1991: TOGA-TAO: A moored array for real-time measurements in the tropical Pacific Ocean. *Bull. Amer. Meteor. Soc.,* **72,** 339–347.

Henry, W. K., 1979: Some aspects of the fate of cold fronts in the Gulf of Mexico. *Mon. Wea. Rev.,* **107,** 1078–1082.

——, 1980: Three late spring fronts in the Caribbean. *Nat. Wea. Dig.,* **5**(1), 18–24.

Hill, J. B., 1969: Temperature variability and synoptic cold fronts in the winter climate of Mexico. Climatological Research Series No. 4, Dept. of Geography, McGill University, Montreal, Canada 71 pp.

Holton, J. R., 1992: *An Introduction to Dynamic Meteorology.* 3d ed. Academic Press, 511 pp.

Horvath, N. C., and W. K. Henry, 1980: Some aspects of cold fronts in Belize. *Nat. Wea. Dig.,* **5**(4), 25–32.

Houze, R. A., Jr., S. G. Geotis, F. D. Marks Jr., and A. K. West, 1981: Winter monsoon convection in the vicinity of North Borneo. Part I: Structure and time variation of the clouds and precipitation. *Mon. Wea. Rev.,* **109,** 1595–1614.

Hsu, S. A., 1993: The Gulf of Mexico—A breeding ground for winter storms. *Mar. Wea. Log,* **37**(2), 4–11.

Huo, Z., D.-L. Zhang, J. Gyakum, and A. Staniforth, 1995: A diagnostic analysis of the superstorm of March 1993. *Mon. Wea. Rev.,* **123,** 1740–1761.

Hurd, W. E., 1929: Northers of the Gulf of Tehuantepec. *Mon. Wea. Rev.,* **57,** 192–194.

Huschke, R. E., Ed., 1959: *Glossary of Meteorology.* Amer. Meteor. Soc., 638 pp.

Hutchinson, T. A., H. B. Bluestein, and K. C. Crawford, 1994: Mesoscale analysis of a pre-frontal trough in the southern Plains. Preprints, *Sixth Conf. on Mesoscale Processes,* Portland, OR, Amer. Meteor. Soc., 292–295.

Jackson, P. L., and D. G. Steyn, 1994: Gap winds in a fjord. Part I: Observations and numerical simulation. *Mon. Wea. Rev.,* **122,** 2645–2665.

Klaus, D., 1973: Las invasiones de aire frio en los tropicos a sotavento de las Montañas Rocallosas (Inversions of cold air in the Tropics on the lee side of the Rocky Mountains). *Geofis. Int.,* **13,** 99–143.

Koch, S. E., M. DesJardins, and P. J. Kocin, 1983: An interactive Barnes objective map analysis scheme for use with satellite and conventional data. *J. Climate Appl. Meteor.,* **22,** 1487–1503.

Kocin, P. J., P. N. Schumacher, R. F. Morales Jr., and L. W. Uccellini, 1995: Overview of the 12–14 March 1993 superstorm. *Bull. Amer. Meteor. Soc.,* **76,** 165–182.

Konrad, C. E., II, 1996: Relationships between the intensity of cold-air outbreaks and the evolution of synoptic and planetary-scale features over North America. *Mon. Wea. Rev.,* **124,** 1067–1083.

Kuo, Y.-H., and R. J. Reed, 1988: Numerical simulation of an explosively deepening cyclone in the eastern Pacific. *Mon. Wea. Rev.,* **116,** 2081–2105.

Lackmann, G. M., and J. E. Overland, 1989: Atmospheric structure and momentum balance during a gap-wind event in Shelikof Strait, Alaska. *Mon. Wea. Rev.,* **117,** 1817–1833.

Ladd, J. W., and W. K. Henry, 1980: An examination of some indicators of frontal passage in coastal Honduras. *Nat. Wea. Dig.,* **5**(3), 2–7.

Lau, K.-M., and C.-P. Chang, 1987: Planetary scale aspects of the winter monsoon and atmospheric teleconnections. *Monsoon Meteorology,* C.-P. Chang and T. N. Krishnamurti, Eds., Oxford University Press, 161–202.

Legeckis, R., 1986: A satellite time series of sea surface temperatures in the eastern equatorial Pacific Ocean, 1982–1986. *J. Geophys. Res.,* **91,** 12 879–12 886.

——, 1988: Upwelling off the Gulfs of Panama and Papagayo in the

tropical Pacific during March 1985. *J. Geophys. Res.*, **93,** 15 485–15 489.
Lessmann, H., 1964: Synoptic and climatological views on rainfall in Central America (especially in El Salvador). *Proc. Symp. on Tropical Meteorology*, Roturua, New Zealand, New Zealand Meteor. Service, 295–305.
Loughe, A. F., C.-C. Lai, and D. Keyser, 1995: A technique for diagnosing three-dimensional ageostrophic circulations in baroclinic disturbances on limited-area domains. *Mon. Wea. Rev.*, **123,** 1476–1504.
Mass, C. F., and D. M. Schultz, 1993: The structure and evolution of a simulated midlatitude cyclone over land. *Mon. Wea. Rev.*, **121,** 889–917.
——, S. Businger, M. D. Albright, and Z. A. Tucker, 1995: A windstorm in the lee of a gap in a coastal mountain barrier. *Mon. Wea. Rev.*, **123,** 315–331.
McBride, J. L., and K. L. McInnes, 1993: Australian southerly busters. Part II: The dynamical structure of the orographically modified front. *Mon. Wea. Rev.*, **121,** 1921–1935.
McBryde, F. W., 1932: A hot norther and terrific squall in eastern Chiapas–April 6, 1928. *Bull. Amer. Meteor. Soc.*, **13,** 130–131.
——, 1942a: Studies in Guatemalan meteorology. Part 1: The climates of southwest Guatemala. *Bull. Amer. Meteor. Soc.*, **23,** 254–263.
——, 1942b: Studies in Guatemalan meteorology. Part 2: Weather types in southwest Guatemala. *Bull. Amer. Meteor. Soc.*, **23,** 400–406.
McCreary, J. P., Jr., H. S. Lee, and D. B. Enfield, 1989: The response of the coastal ocean to strong offshore winds: With application to circulations in the Gulfs of Tehuantepec and Papagayo. *J. Mar. Res.*, **47,** 81–109.
McInnes, K. L., and J. L. McBride, 1993: Australian southerly busters. Part I: Analysis of a numerically simulated case study. *Mon. Wea. Rev.*, **121,** 1904–1920.
Mecikalski, J. R., and J. S. Tilley, 1992: Cold surges along the Front Range of the Rocky Mountains: Development of a classification scheme. *Meteor. Atmos. Phys.*, **48,** 249–271.
Moore, J. T., and G. E. VanKnowe, 1992: The effect of jet-streak curvature on kinematic fields. *Mon. Wea. Rev.*, **120,** 2429–2441.
Mosiño Alemán, P. A., and E. García, 1974: The climate of Mexico. *World Survey of Climatology*, Vol. 11, *Climates of North America*, R. A. Bryson and F. K. Hare, Eds., Elsevier, 345–404.
Myers, V. A., 1964: A cold front invasion of southern Venezuela. *Mon. Wea. Rev.*, **92,** 513–521.
National Weather Service, 1994: Superstorm of March 1993: March 12–14, 1993. Natural Disaster Survey Rep., U.S. Dept. of Commerce, 152 pp.
Newton, C. W., 1950: Structure and mechanism of the prefrontal squall line. *J. Meteor.*, **7,** 210–222.
——, 1965: Variations in structure of subtropical current system accompanying a deep polar outbreak. *Mon. Wea. Rev.*, **93,** 101–110.
Orlanski, I., 1975: Rational subdivision of scales for atmospheric processes. *Bull. Amer. Meteor. Soc.*, **56,** 527–530.
——, and J. P. Sheldon, 1995: Stages in the energetics of baroclinic systems. *Tellus*, **47A,** 605–628.
Overland, J. E., and B. A. Walter Jr., 1981: Gap winds in the Strait of Juan de Fuca. *Mon. Wea. Rev.*, **109,** 2221–2233.
Palmer, C. E., 1951: Tropical meteorology. *Compendium of Meteorology*, T. F. Malone, Ed., Amer. Meteor., Soc., 859–880.
Parmenter, F. C., 1970: A ''tehuantepecer.'' *Mon. Wea. Rev.*, **98,** 479.
——, 1976: A Southern Hemisphere cold front passage at the equator. *Bull. Amer. Meteor. Soc.*, **57,** 1435–1440.
Peixoto, J. P., and A. H. Oort, 1992: *Physics of Climate*. American Institute of Physics, 520 pp.
Pond, S., and G. L. Pickard, 1983: *Introductory Dynamical Oceanography*. 2d ed. Pergamon Press, 329 pp.
Portig, W. H., 1959: Air masses in Central America. *Bull. Amer. Meteor. Soc.*, **40,** 301–304.
——, 1965: Central American rainfall. *Geogr. Rev.*, **55,** 68–90.
——, 1976: The climate of Central America. *World Survey of Climatology*, Vol. 12, *Climates of Central and South America*, W. Schwerdtfeger, Ed., Elsevier, 405–478.
Prohaska, F., 1976: The climate of Argentina, Paraguay, and Uruguay. *World Survey of Climatology*, Vol. 12, *Climates of Central and South America*, W. Schwerdtfeger, Ed., Elsevier, 13–112.
Ramage, C. S., 1971: *Monsoon Meteorology*. Academic Press, 296 pp.
Ramp, S. R., P. F. Jessen, K. H. Brink, P. P. Niiler, F. L. Daggett, and J. S. Best, 1991: The physical structure of cold filaments near Point Arena, California, during June 1987. *J. Geophys. Res.*, **96,** 14 859–14 883.
Ratisbona, L. R., 1976: The climate of Brazil. *World Survey of Climatology*, Vol. 12, *Climates of Central and South America*, W. Schwerdtfeger, Ed., Elsevier, 219–294.
Reding, P. J., 1992: The Central American cold surge: An observational analysis of the deep south-ward penetration of North American cold fronts. M.S. thesis, Dept. of Meteorology, Texas A&M University, 177 pp.
Reed, T. R., 1931: Gap winds of the Strait of Juan de Fuca. *Mon. Wea. Rev.*, **59,** 373–376.
Richwien, B. A., 1980: The damming effect of the southern Appalachians. *Nat. Wea. Dig.*, **5**(1), 2–12.
Riehl, H., 1954: *Tropical Meteorology*. McGraw-Hill, 392 pp.
Roden, G. I., 1961: On the wind driven circulation in the Gulf of Tehuantepec and its effect upon surface temperatures. *Geofis. Int.*, **1**(3), 55–76.
Rottman, J. W., and J. E. Simpson, 1989: The formation of internal bores in the atmosphere: A laboratory model. *Quart. J. Roy. Meteor. Soc.*, **115,** 941–963.
Sanders, F., 1955: An investigation of the structure and dynamics of an intense surface frontal zone. *J. Meteor.*, **12,** 542–552.
——, and C. A. Doswell III, 1995: A case for detailed surface analysis. *Bull. Amer. Meteor. Soc.*, **76,** 505–521.
Schoenberger, L. M., 1984: Doppler radar observation of a landbreeze cold front. *Mon. Wea. Rev.*, **112,** 2455–2464.
Schumann, S. A., J. Moser, G. A. Johnson, N. D. Walker, and S. A. Hsu, 1995: An overview of a strong winter low in the Gulf of Mexico 12–13 March 1993. *Nat. Wea. Dig.*, **20,** 11–25.
Shapiro, M. A., 1984: Meteorological tower measurements of a surface cold front. *Mon. Wea. Rev.*, **112,** 1634–1639.
Simpson, J. E., 1987: *Gravity Currents: In the Environment and the Laboratory*. Ellis Horwood, 244 pp.
Skamarock, W. C., J. B. Klemp, and R. Rotunno, 1996: The diffraction of Kelvin waves and bores at coastal bends. *J. Atmos. Sci.*, **53,** 1327–1337.
Smith, R. K., and M. J. Reeder, 1988: On the movement and low-level structure of cold fronts. *Mon. Wea. Rev.*, **116,** 1927–1944.
——,——, N. J. Tapper, and D. R. Christie, 1995: Central Australian cold fronts. *Mon. Wea. Rev.*, **123,** 16–38.
Snow, J. W., 1976: The climate of northern South America. *World Survey of Climatology*, Vol. 12, *Climates of Central and South America*, W. Schwerdtfeger, Ed., Elsevier, 295–404.
Spinden, H. J., 1928: Central America rainfall map. *Geogr. Rev.*, **18,** 660–661.
Stumpf, H. G., 1975a: Satellite detection of upwelling in the Gulf of Tehuantepec, Mexico. *Mar. Wea. Log*, **19,** 71–74.
——, 1975b: Satellite detection of upwelling in the Gulf of Tehuantepec, Mexico. *J. Phys. Oceanogr.*, **5,** 383–388.
——, and R. V. Legeckis, 1977: Satellite observations of mesoscale eddy dynamics in the eastern tropical Pacific Ocean. *J. Phys. Oceanogr.*, **7,** 648–658.
Suomi, V. E, R. Fox, S. S. Limaye, and W. L. Smith, 1983: McIDAS III: A modern interactive data access and analysis system. *J. Climate Appl. Meteor.*, **22,** 766–778.
Taljaard, J. J., 1972: Synoptic meteorology of the Southern Hemisphere. *Meteorology of the Southern Hemisphere*, C. W. Newton, Ed., Amer. Meteor. Soc., 139–213.
Tepper, M., 1950: A proposed mechanism of squall lines: The pressure jump line. *J. Meteor.*, **7,** 21–29.

Trasviña, A., E. D. Barton, J. Brown, H. S. Velez, P. M. Kosro, and R. L. Smith, 1995: Offshore wind forcing in the Gulf of Tehuantepec, Mexico: The asymmetric circulation. *J. Geophys. Res.,* **100,** 20 649–20 663.

Trenberth, K. E., 1992: Global analyses from ECMWF and atlas of 1000 to 10 mb circulation statistics. NCAR Tech. Note NCAR/TN-373+STR, 191 pp.

Trewartha, G. T., 1966: *The Earth's Problem Climates.* University of Wisconsin Press, 334 pp.

Tyle, K. R., 1995: Intense surface anticyclogenesis: Climatology and composite/individual case studies. M.S. thesis, Dept. of Atmospheric Science, State University of New York at Albany, 252 pp.

Uccellini, L. W., and D. R. Johnson, 1979: The coupling of upper and lower tropospheric jet streaks and implications for the development of severe convective storms. *Mon. Wea. Rev.,* **107,** 682–703.

——, P. J. Kocin, R. S. Schneider, P. M. Stokols, and R. A. Dorr, 1995: Forecasting the 12–14 March 1993 superstorm. *Bull. Amer. Meteor. Soc.,* **76,** 183–199.

Walker, N. D., 1993: A preliminary look at cyclogenesis in Gulf of Mexico during the March 1993 blizzard. *Mar. Wea. Log,* **37**(2), 8–9.

Wang, D.-P., 1987: The strait surface outflow. *J. Geophys. Res.,* **92,** 10 807–10 825.

Weatherwise, 1963: A brief climatography of Mexico. *Weatherwise,* **16,** 230–236.

——, 1995: Superstorm success. *Weatherwise,* **48**(3), 18–24.

Woodruff, S. D., R. J. Slutz, R. L. Jenne, and P. M. Steurer, 1987: A Comprehensive Ocean–Atmosphere Data Set. *Bull. Amer. Meteor. Soc.,* **68,** 1239–1250.

Wu, M. C., and J. C. L. Chan, 1995: Surface features of winter monsoon surges over South China. *Mon. Wea. Rev.,* **123,** 662–680.